Assessing Groundwater Storage Changes Using Remote Sensing–Based Evapotranspiration and Precipitation at a Large Semiarid Basin Scale

MUSTAFA GOKMEN, ZOLTAN VEKERDY, MACIEK W. LUBCZYNSKI, AND JORIS TIMMERMANS

Department of Water Resources, Faculty of Geo-Information Science and Earth Observation (ITC), University of Twente, Enschede, Netherlands

OKKE BATELAAN

Department of Hydrology and Hydraulic Engineering, Vrije Universiteit Brussel, Brussels, Belgium, and School of the Environment, Flinders University, Adelaide, South Australia, Australia

WOUTER VERHOEF

Department of Water Resources, Faculty of Geo-Information Science and Earth Observation (ITC), University of Twente, Enschede, Netherlands

(Manuscript received 19 October 2012, in final form 10 July 2013)

ABSTRACT

A method is presented that uses remote sensing (RS)-based evapotranspiration (ET) and precipitation estimates with improved accuracies under semiarid conditions to quantify a spatially distributed water balance, for analyzing groundwater storage changes due to supplementary water uses. The method is tested for the semiarid Konya basin (Turkey), one of the largest endorheic basins in the world. Based on the spatially distributed water balance estimation, the mean irrigation for croplands was 308 mm yr^{-1}, which corresponds to a total reduction of 2270 million cubic meters per year (10^6 m^3 yr^{-1}, or MCM yr^{-1}) in the groundwater storage during the study period 2005–09. The storage change estimated as the residual of the spatially distributed water balance was confirmed by the volume change calculated from groundwater table observations. To obtain an improved precipitation distribution, the monthly Tropical Rainfall Measuring Mission (TRMM) rainfall product was assessed. After a bias removal, TRMM data were combined with the snow water equivalent estimated by a multivariate analysis using snow gauge observations, the Moderate Resolution Imaging Spectroradiometer (MODIS) snow cover product, and the digital elevation model. With respect to the distribution of ET, the standard SEBS and the soil moisture integrated SEBS-SM models were compared; SEBS-SM proved to better reflect the water-limited evapotranspiration regime of semiarid regions. The RS-based distributed water balance calculation as presented in this study can be applied in other large basins, especially in semiarid and arid regions. It is capable of estimating spatially distributed water balances and storage changes, which otherwise, by ground-based point measurements, would not be feasible.

1. Introduction

In arid and semiarid regions, characterized by low precipitation (P) and high potential evapotranspiration (PET), accurate knowledge of P, of actual evapotranspiration (ET), and the balance between the two ($P - ET$), as well as their spatiotemporal distribution, is essential for sustainable management of the scarce water resources. In such dry, water-limited regions, groundwater (GW) is often the only reliable water resource.

Since the 1950s, groundwater resources of many arid and semiarid areas have been affected by a number of nonclimatic forcings, such as heavy groundwater abstraction for irrigation purpose. These often resulted in lowering of the groundwater table, reflecting a loss of aquifer storage (Green et al. 2011). If groundwater abstraction exceeds the net groundwater recharge

Corresponding author address: Mustafa Gokmen, Department of Water Resources, Faculty of Geo-Information Science and Earth Observation (ITC), University of Twente, P.O. Box 217, 7500 AE Enschede, Netherlands.
E-mail: mustaf.gokmen@gmail.com

DOI: 10.1175/JHM-D-12-0156.1

over prolonged periods, persistent groundwater depletion occurs (Gleeson et al. 2010). For such cases, Wada et al. (2012) explicitly use the term ''nonrenewable groundwater abstraction.'' The semiarid Konya basin in central Anatolia (Turkey), which is one of the biggest endorheic basins in the world, is a typical example of groundwater resources under strong anthropogenic pressure. Over the last few decades, the basin experienced huge groundwater abstraction for irrigation, which caused a hydraulic head decline of $\sim 1\,\mathrm{m\,yr^{-1}}$ (Bayari et al. 2009).

Establishing the spatial and temporal distribution of hydrological fluxes using remote sensing (RS) methods has been the focus of many recent research efforts (McCabe et al. 2008) because of their potential to provide spatially continuous and temporally recurrent estimates over regional to global scales (Alsdorf and Lettenmaier 2003). Precipitation is regularly retrieved from multisensor microwave and infrared data using a variety of techniques (e.g., Joyce et al. 2004). One of the recent datasets is the Tropical Rainfall Measuring Mission (TRMM) Multisatellite Precipitation Analysis (TMPA), which is designed to combine precipitation estimates from various satellite systems, as well as land surface precipitation gauge analyses where possible (Huffman et al. 2007). Furthermore, evapotranspiration can be determined from RS-based solutions of the surface energy balance (Su et al. 2005). Such global ET products from the RS retrievals are becoming increasingly available (Ghilain et al. 2011; Su et al. 2010; Vinukollu et al. 2011).

However, the capabilities of RS to ''look below the ground surface'' and to detect the groundwater conditions directly are limited (Green et al. 2011). One of the major exceptions to this is the satellite-based observations of Earth's gravity field: changes in total surface and subsurface storage can be derived using gravity anomaly measurements with the Gravity Recovery and Climate Experiment (GRACE) satellites (Swenson and Wahr 2002). However, with spatial resolution of 400–500 km this technique can provide change of groundwater storage over regions of about $150\,000\,\mathrm{km^2}$ or larger at 10-day to monthly temporal scales (Wahr et al. 2006; Yeh et al. 2006). Therefore, in smaller regions or at a basin scale, where most of the water resource, meteorological, agricultural, and natural hazard investigations are carried out, satellite gravimetry is often not applicable. An alternative is to infer changes in the water storage (ΔS) by estimating the difference between P, ET, and runoff R (Brunner et al. 2004), integrating remote sensing retrievals and ground measurements. Tang et al. (2010) followed such a methodology to assess the temporal variations of terrestrial ΔS from surface P observations, satellite-based ET estimation, and gauge R measurements for two major river basins, and found that human influences have extensively altered the natural hydrological processes and seasonal ΔS in the study area. Differently, exploring the feasibility of entirely RS-based water budget for a ground-data constrained basin, Armanios and Fisher (2013) concluded that such a purely RS-based methodology is more appropriate for long-term water resources assessment (e.g., annual scale) than ''instantaneous'' or short-term assessment.

Estimates based on models or reanalysis (combinations of models and observations) are other methods to estimate the terrestrial water storage or the changes in water storage (ΔS). However, Tang et al. (2010) note that the main limitation in using the modeled terrestrial water storage is at the river basin scale, where water management (e.g., man-made reservoirs and irrigation water withdrawals) substantially affects the land surface hydrological dynamics, as these effects are not represented in most land surface models.

In this study, we propose a relatively simple method that integrates RS-based seasonal and yearly P and ET estimates with minimum ground data for assessing water balance and storage changes in a spatially distributed manner. The methodology is tested and applied for the large semiarid Konya basin (approximately $54\,000\,\mathrm{km^2}$) where 1) both human activities (agriculture) and natural ecosystems are highly groundwater dependent and 2) the limited surface runoff is managed through man-made reservoirs for supplying irrigation. More specifically, this study aims at

1) Quantifying by remote sensing the spatiotemporal P and ET fluxes with improved accuracy under semiarid conditions at the large basin scale combining them with field data where needed and available,
2) Analyzing the spatiotemporal water balance to assess the water availability (surface runoff), consumptive water use (irrigation), GW storage changes and GW discharge using the spatially distributed, yearly P, ET fluxes, and
3) Assessing the consistency and errors of RS-based water balance and storage change estimates with groundwater observations.

2. Materials and methods

a. The study area

The Konya basin is located in central Anatolia, Turkey, between 36.8°N, 31.0°E and 39.5°N, 35.1°E. The basin covers a surface area of about $54\,000\,\mathrm{km^2}$, with elevations ranging from 900 to 3500 m above mean sea level (MSL) (Fig. 1). There are extensive plains in the central and downstream parts of the basin, which make the Konya

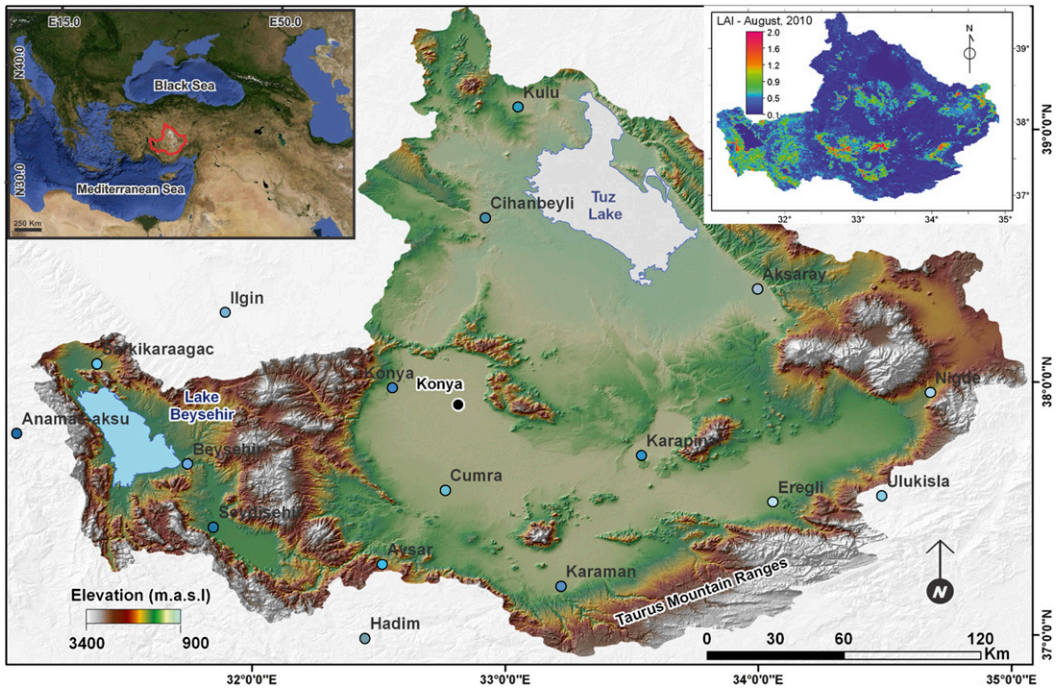

FIG. 1. The (top left) geographic location, (top right) vegetation distribution (leaf area index), and (bottom) SRTM-based elevation map with the locations of the meteorological stations of the study area.

basin one of the most important agricultural regions of Turkey. There are two large lakes in the basin: the hypersaline Tuz Lake in the northern, downstream part and the freshwater Lake Beysehir in the western upstream part. Besides, numerous smaller, dominantly groundwater-fed, fresh or brackish water bodies and wetlands are present in the mid- and downstream areas, some of which have dried out in the last decades.

The Konya basin has a typical arid to semiarid climate with an average yearly precipitation of 380 mm [unpublished data from State Hydraulic Works (DSI)]. The summers are hot and dry (maximum temperature reaching ~40°C) whereas winters are cold and wet (minimum temperature may go down to about −20°C). While the southwestern upstream part shows a warmer and wetter Mediterranean character, the rest of the basin has a drier, continental climate, isolated from the moderating effect of the Mediterranean Sea by the Taurus Mountains in the south.

The land cover in the basin shows a strong contrast between intensively irrigated agricultural lands and the sparsely vegetated steppe areas covering the mid- and downstream plains, where natural vegetation is dominated by *Artemisia* grasses (Fontugne et al. 1999). Generally, all these steppe vegetation types are nonwoody plants with relatively small canopy height (20–40 cm) and shallow rooting depths. The adaptation methods of the natural vegetation to drought stress differ between the downstream area, where the groundwater is shallow and saline, and the rest of the region, where the groundwater table is at 35–50-m depths. In the mountainous parts in the south and southwest of the basin, forest and shrub are dominant.

The distribution of agricultural crops (based on data from 2007) is 38% cereals, 28% sugar beet, 19% vegetables, 13% fruits, and 2% other (unpublished data from DSI). Groundwater is the main source of water for irrigation and is abstracted from the Neogene aquifer by 50- to 250-m-deep wells (Bayari et al. 2009), although some surface water is also utilized.

b. Estimating precipitation and evapotranspiration by remote sensing

1) SPATIOTEMPORAL DISTRIBUTION OF PRECIPITATION

To quantify precipitation we estimated rainfall and snow water equivalent (SWE) separately, combining RS-based approaches and gauge measurements. The flowchart (Fig. 2) explains the determination of the rainfall, the SWE, and the total precipitation. The yearly precipitation was calculated per hydrological year (from 1 October to 30 September next year) and per season (the wet season covers 6 months between 1 October and 31 March, and the dry season covers 6 months between 1 April and 30 September).

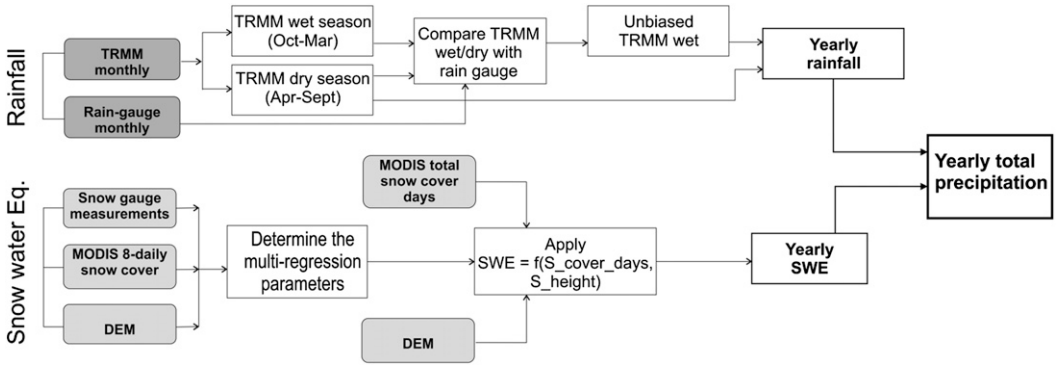

FIG. 2. Flowchart for determining the yearly rainfall, the snow water equivalent (SWE), and the total precipitation. All fluxes are in mm yr^{-1}.

To estimate the rainfall distribution, we used the monthly product of the Tropical Rainfall Measuring Mission (TRMM-3B43) combined with local rain gauge measurements. The TRMM algorithm combines four independent sources: 1) the monthly average TRMM Microwave Imager (TMI) estimate, 2) the monthly average Special Sensor Microwave Imager (SSM/I) estimate, 3) the pentad-average adjusted merged-infrared (IR) estimate, and 4) the monthly accumulated Climate Assessment and Monitoring System (CAMS) and Global Precipitation Climatology Centre (GPCC) rain gauge analysis. The TRMM $25 \times 25\,km^2$ gridded estimates extend from 50°S to 50°N (http://mirador.gsfc.nasa.gov/collections/TRMM_3B43__006.shtml) and have temporal resolution corresponding to a calendar month.

Pan et al. (2008) indicated that TRMM products have large differences as compared to ground observations at short time intervals (3 hourly) but the discrepancies become smaller as the aggregation time increases. They also reported a positive bias of the TRMM product. To ensure improved spatiotemporal rainfall estimation for the Konya basin, we first aggregated the monthly TRMM data to wet and dry season rainfalls, compared them with the gauge observations, and, where necessary, carried out a linear rescaling for correcting the bias as described by Pan et al. (2008). Also, we resampled the originally 25-km spatial resolution to 1-km resolution using bicubic interpolation in order to match it with the resolution of ET flux for the spatially distributed water balance analysis.

It should be highlighted that neither the TRMM rainfall product nor the rain gauge observations (as they are not located at higher altitudes) sufficiently captures the snowfall contribution to the total precipitation. In the TRMM-3B43 product document it is stated that the snowfall regions are identified through the use of Advanced Microwave Sounding Unit A (AMSU-A) measurements and falling snow is assigned a rate of $0.1\,mm\,h^{-1}$ (Huffman and Bolvin 2013). Because of the coarse resolution of AMSU-A (50 km at nadir; Prigent et al. 2005) and the mountainous topography of the study area, the TRMM-3B43 product was considered to be insufficient to detect snowfall contribution in the Konya basin.

Direct, in situ measurements and RS estimates of SWE (Serreze et al. 1999) are extremely limited (Tang et al. 2010). To date, most robust global data records for SWE are derived by satellite-based microwave sensor systems such as the Scanning Multichannel Microwave Radiometer (SMMR), the SSM/I, and the Advanced Microwave Scanning Radiometer for Earth Observing System (AMSR-E; Muskett 2012). However, satellite-based SWE data and applications usually cover high latitudes (65°N and higher) and relatively flat terrains (e.g., Biancamaria et al. 2008; Derksen et al. 2010; Chang et al. 2005), so those are not easily applicable for the Konya basin. Therefore, to estimate the spatiotemporal SWE in the Konya basin, we applied a multivariate linear regression approach. As dependent variables we used the available ground measurements from snow gauges within the basin (Fig. 3). As independent variables we considered the total amount of snow cover days from the 8-day snow cover product of the Moderate Resolution Imaging Spectroradiometer (MODIS; MOD10A2) as well as the elevation of the location of snow measurements obtained from the digital elevation model (DEM). After determining the multivariate regression parameters for each year separately, we applied them using the inputs of total snow cover days from MODIS and DEM of the basin to estimate the yearly total SWE distribution for each year during the study period (2005–09).

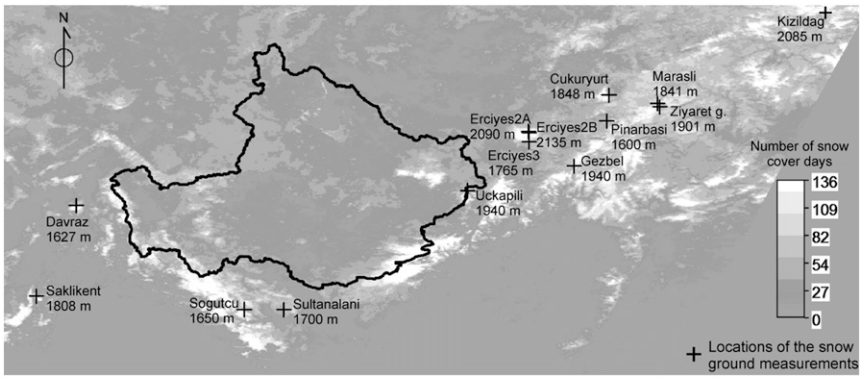

FIG. 3. The locations and altitudes (m MSL) of the ground snow measurements around the Konya basin. The background image shows the total amount of snow cover days from MOD10A2 product in 2005–06 (between October and April).

The data of in situ snow measurements were obtained from DSI (unpublished data). The snow measurements were conducted on monthly basis (Fig. 3) by DSI between October and May, recording the average snow depth, snow water equivalent, and snow density values. In the multivariate regression analysis, we used the maximum snow depth and corresponding SWE values (usually occur in April/May) as the yearly SWE values, assuming the major snow melting occurs in spring and snow mainly stays in the solid state throughout the winter seasons.

Finally, the total yearly precipitation was estimated by summing the bias-corrected yearly rainfall and the yearly SWE.

2) SPATIOTEMPORAL DISTRIBUTION OF EVAPOTRANSPIRATION

(i) Actual evapotranspiration

RS-based surface energy balance models are increasingly used to determine the distribution of evapotranspiration from field to global scales. The physically based and single source Surface Energy Balance System model (SEBS; Su 2002) is one of the widely used surface energy balance models, which has been applied in many regional to global studies (Ma et al. 2012; Pan et al. 2012; Vinukollu et al. 2011; Jin et al. 2009; Pan et al. 2008; Ma et al. 2007; Oku et al. 2007; Jia et al. 2003). The SEBS model estimates actual evapotranspiration using RS retrievals and in situ measurements to define incoming surface radiation, surface skin temperature, surface meteorology, and surface and vegetation properties (Su et al. 2005). Latent heat flux, or equivalently evapotranspiration, is estimated considering the surface energy balance and the evaporative fraction.

Comparing three process-based models (i.e., SEBS, Penman–Monteith, and Priestley–Taylor) to ET at the global scale, Vinukollu et al. (2011) concluded that all of them appear to underrepresent the sensitivity to soil moisture over water-limited regions and because of that overestimate ET. To handle this problem, in this study we used besides SEBS also a modified version of SEBS called SEBS-SM (Gokmen et al. 2012), which additionally integrates soil moisture data in SEBS through incorporating a water stress index in a modified definition of the aerodynamic resistance. Its performance was tested by Gokmen et al. (2012) through comparing it with ground-based data measured by four Bowen ratio stations. The results indicated not only a clear improvement in the heat flux estimations for the case of sparse vegetation ($70\,W\,m^{-2}$ reduction in RMSE) but also an overall improvement of the model performance ($40\,W\,m^{-2}$ reduction in RMSE).

Figure 4 provides a flowchart of explaining acquisition of daily, monthly, and yearly ET by SEBS-SM. The SEBS-SM was run on a daily interval using MODIS input data with 1-km spatial resolution on thermal bands. The model output had some missing days due to either the cloud coverage or unreliable data masked out by the quality control of the MODIS team on the input variables such as emissivity or land surface temperature (T_0). For filling the ET data gaps, we implemented a monthly average compositing by dividing the sum of the available daily ET estimates by the number of days with available ET estimates for each pixel. Afterward, the monthly total ET values were calculated by multiplying the average daily ET (for the month) by 30 days except for the three winter months from December to February when the monthly total ET was estimated by multiplying the average daily ET by 15, considering that 1) the maximum available cloud-free data were rarely above 15 unlike the other months and 2) occasions of day long cloud-casting or inversions that minimize evaporation

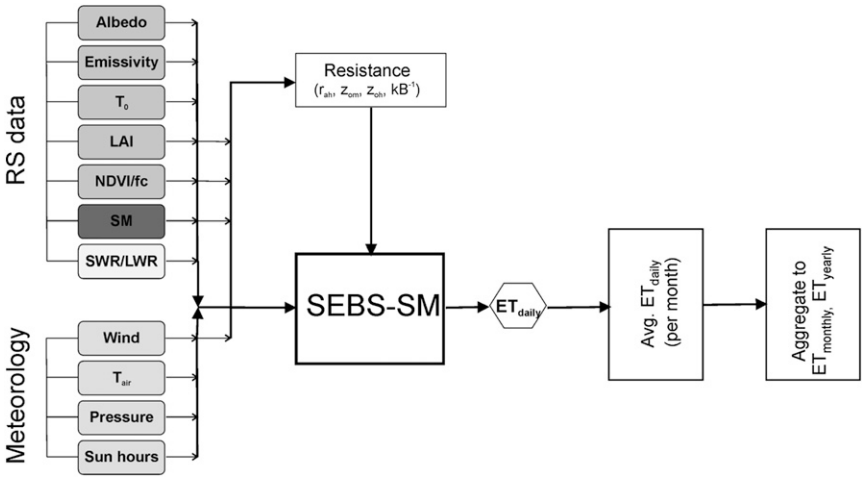

FIG. 4. Input data for SEBS-SM and flowchart of aggregating ET.

were more common in winter months due to dominance of frontal weather systems and continental climate.

To retrieve the necessary input parameters for SEBS-SM, we used MODIS land products (https://lpdaac.usgs.gov/products/modis_products_table) and AMSR-E soil moisture products (Owe et al. 2008) as listed in Table 1. The study covered the period between 2005 and 2009.

In addition to the RS data, the necessary meteorological forcing data (Fig. 4) were obtained from the Turkish Meteorological Service for the 18 stations located in and around the basin (Fig. 1). The point measurements of the stations were spatially interpolated using the natural neighbor interpolation. With respect to instantaneous and daily air temperature, the local lapse rates were calculated for the mountainous areas and integrated (based on a DEM) in the interpolation of air temperature data.

Finally, the downwelling shortwave and longwave radiation flux (R_{swd} and R_{lwd}), boundary layer height, and dewpoint temperature at 2-m height were retrieved from the high-resolution gridded European Centre for Medium-Range Weather Forecasts (ECMWF) Interim Re-Analysis (ERA-Interim) dataset (http://data-portal.ecmwf.int/).

(ii) Potential evapotranspiration

In addition to actual ET, we also used the data of potential evapotranspiration in this study, which is a representation of the atmospheric demand for evapotranspiration. PET data were used in determining the distribution of water limitation in the region based on the criterion for the water-limited environments defined by Parsons and Abrahams (1994). The spatio-temporal PET distribution of the Konya basin was obtained using the class-A pan evaporation data from the 18 meteorological stations (Fig. 1) and the simplified formula by Snyder et al. (2005).

c. Spatially distributed water balance

The water balance equation for a basin with coinciding surface and groundwater divides can be written in a simple form as Eq. (1) (Penck 1896; Pagano and Sorooshian 2006):

$$P - \mathrm{ET} - R \pm \Delta S = 0, \tag{1}$$

where P is precipitation, ET is actual evapotranspiration, R is total runoff, and ΔS is the change in storage.

Figures 5a and 5b present the conceptual model of the hydrological fluxes in the Konya basin. The Taurus

TABLE 1. The details of the RS data used in the study.

Name of Sensor	Product code	Product name	Spatial resolution	Temporal resolution	Temporal coverage
MODIS	MCD43A3	Albedo	500 m	16 days	Feb 2000–
MODIS	MOD11A1	Emissivity and land surface temperature	1000 m	Daily	Mar 2000–
MODIS	MCD15A2	Leaf area index	1000 m	8 days	Jul 2002–
MODIS	MOD13A2	NDVI	1000 m	16 days	Feb 2000–
AMSR-E		Surface soil moisture	~25 km	2–3 days	Jun 2002–Oct 2011

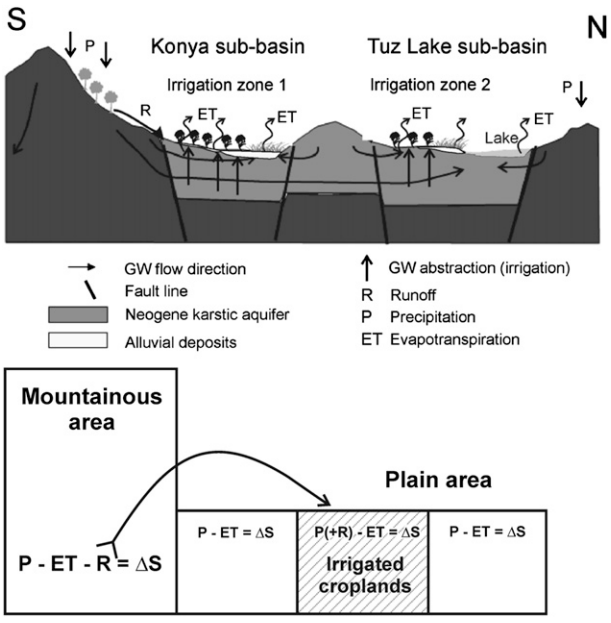

FIG. 5. (top) Conceptual model of the Konya basin [modified after Bayari et al. (2009) and Naing (2011)] and (bottom) water balance equations for the (left) mountainous area and (right) plain area.

Mountains in the south and southwest are the main water source areas, where high rainfall and snowmelt feed the ephemeral rivers and recharge the aquifer. Because of the well-developed karst geology, (semi)arid climate, and the huge plain areas in the mid- and downstream parts, the Konya basin has no well-established drainage network. The water from the ephemeral rivers is either stored in the reservoirs to facilitate irrigation or feeds the groundwater along the footslopes of the mountains. The basin is hydrologically closed, meaning that the horizontal fluxes of surface and groundwater are retained in the basin terminating at the Tuz Lake in the north (Bayari et al. 2009). The evapotranspiration constitutes the only outflux from the basin and controls salinization of the surface water bodies such as the hypersaline Tuz Lake (Bayari et al. 2009). Considering that the Konya basin is closed, its water balance equation can be simplified as

$$\Delta S = P - \mathrm{ET}. \tag{2}$$

However, the objective of this study is to develop a spatially distributed water balance. The basin consists of two major units with different hydrological regimes: 1) the mountainous parts of the basin produce runoff that is transferred to 2) the central plains and used for irrigation in extensive croplands (surrounded by nonirrigated croplands and natural steppe vegetation). Figure 5b illustrates schematically flux exchange between these two subregions and their simplified water balance equations.

Although the abstracted GW is the main source of water supply for irrigation (Bayari et al. 2009) in the plains, the surface water (SW) contributes with ~15%–30% to the irrigation demand in the plains area (unpublished data from DSI) through SW transfer from the mountainous area. This water is first stored in reservoirs at the mountain footslopes and later transferred to the plains area through a system of canals with monitored discharge. Based on the conceptual model in Fig. 5b, Fig. 6 shows the flowchart of redistribution of the surface runoff R generated in the wet season as surface water irrigation in the dry season and then determining the spatially distributed yearly water balance in the Konya basin. After estimating the wet (1 October–31 March) and dry (1 April–30 September) period P and ET fluxes (step 1 in Fig. 6), to estimate runoff (R) from the mountainous area we introduced a mean surface water ratio [$\mathrm{SW_{ratio}}$, Eq. (3)] using P_{wet} and $\mathrm{ET_{wet}}$ data (2005–09) of two subbasins, Beysehir and Yesildere (step 2 in Fig. 6). Once the $\mathrm{SW_{ratio}}$ was defined (average of the two subbasins), the amount of SW available for the water transfer was estimated by multiplying $\mathrm{SW_{ratio}}$ with the $P_{\mathrm{wet}} - \mathrm{ET_{wet}}$ values in the source areas. The SW source areas were determined based on the condition $P_{\mathrm{wet}} - \mathrm{ET_{wet}} > 0$, typically in mountainous areas with altitude >1800 m MSL.

$$\text{SW ratio} = \frac{\sum R_{\mathrm{outflow}}}{\sum P_{\mathrm{wet}} - \sum \mathrm{ET_{wet}}}. \tag{3}$$

Then, in the next step (step 3), the estimated SW amount was deducted from the P_{wet} source pixels in the mountainous area and distributed (for the specific year) over the P_{dry} ''irrigated land'' pixels in the plain areas (Fig. 5) identified on the land cover map in the form of extra precipitation (representing SW irrigation). Next, the modified P_{wet} and P_{dry} were summed to calculate the final redistributed total P, which incorporated the transfer of the SW generated from the wet period into the dry period when surface water irrigation was provided (step 4). Finally, a spatially distributed yearly water balance was obtained by subtracting the yearly total ET from the redistributed yearly total P (Fig. 6).

Afterward, to assess the budget closure at the locations (pixels) of GW observation wells, ΔS_{RS} estimated from RS ($P \pm R - \mathrm{ET}$) were compared with the ΔS_{GW} calculated based on yearly groundwater level observations. However, to enable such a comparison, it was necessary to bring both to the same terms. For instance, the water balance ($P \pm R - \mathrm{ET}$) for a particular pixel (over land surface) corresponds to the total subsurface

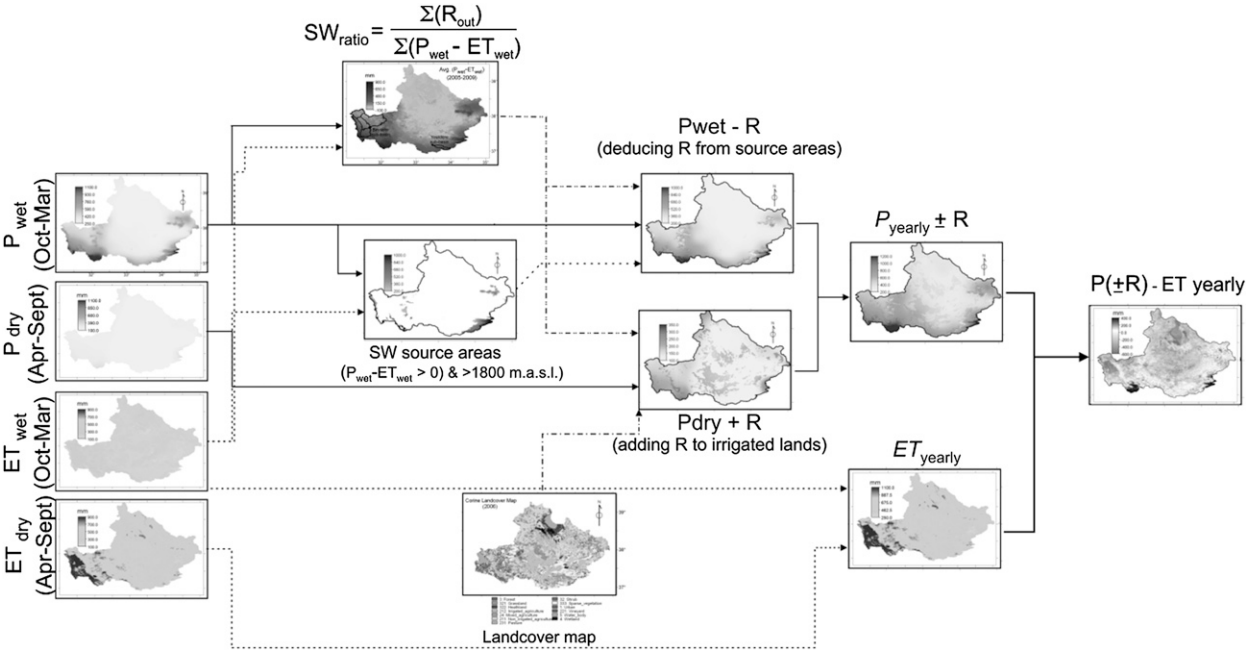

FIG. 6. Flowchart for determining the yearly water balance in the Konya basin.

change in water storage, both in the unsaturated zone (ΔS_{SM}) and groundwater (ΔS_{GW}) ($\Delta S_{RS} = \Delta S_{SM} + \Delta S_{GW}$). Therefore, to minimize the effect of changes in the soil moisture on the total storage change, the spatially distributed P, ET fluxes, and water balance were calculated for an extended period of 5 yr between 2005 and 2009 (i.e., assuming that $\Delta S_{SM} \approx 0$ and $\Delta S_{RS} \approx \Delta S_{GW}$). On the other hand, we calculated ΔS_{GW} values (effective groundwater loss from aquifer) based on the GW level observations and the estimated specific yield of the aquifer. Because of the karstic formation of the aquifers and equipment limitation, it was not possible to parameterize the specific yield experimentally. Hence, we assumed a conservative range of 0.05–0.20 based on literature overview (Johnson 1967; Bolster et al. 2001).

3. Results

a. Spatial distribution of precipitation

Figures 7a and 7b show the comparison of the 6-monthly sums of the TRMM rainfall product and the ground-based rain gauge measurements in dry (April–September) and wet (October–March) seasons, in the Konya basin. In both seasons, a significant linear relationship ($p < 0.001$) is confirmed, and a consistent positive bias of around 80 mm by TRMM is observed for the wet seasons (2005–09). Furthermore, the correlation for the wet season ($r^2 = 0.58$) was higher compared to the dry season ($r^2 = 0.39$). Figure 7c shows the yearly average rainfall distribution after removing the bias in the wet season (2005–09). The rainfall in mountainous area (outside the polygon in Fig. 7c) is on the order of 1000 mm yr^{-1} or more toward the higher parts of the mountains, whereas in the plain (inside the polygon in Fig. 7c) the rainfall is quite uniform, ranging from 250 to 300 mm yr^{-1}.

Figure 8 shows the results of multiregression parameters and the yearly SWE for the year 2008 as an example because the analysis was carried out separately for each year during the study period. Figures 8a and 8b show the relationship between SWE and elevation and total snow cover days, respectively. Although the coefficients of determination (R^2) were in similar range for both linear relationships, the one with total snow cover days had higher R^2 value ($R^2 = 0.65$). On the other hand, a multiregression model combining the two variables explained the variation of SWE better than the individual linear models, with R^2 increased to 0.68. As a result, Fig. 8c shows the distribution of the yearly SWE in the Konya basin obtained from the multiregression model and indicates values of about 300 mm in the mountainous upstream parts of the basin (>2000 m MSL). Finally, Fig. 8d shows the distribution of the yearly total precipitation in the Konya basin, which was obtained by summing the yearly rainfall and SWE.

b. Spatial distribution of evapotranspiration

Figure 9 shows the comparison of the average yearly ET estimated by the original SEBS and the modified

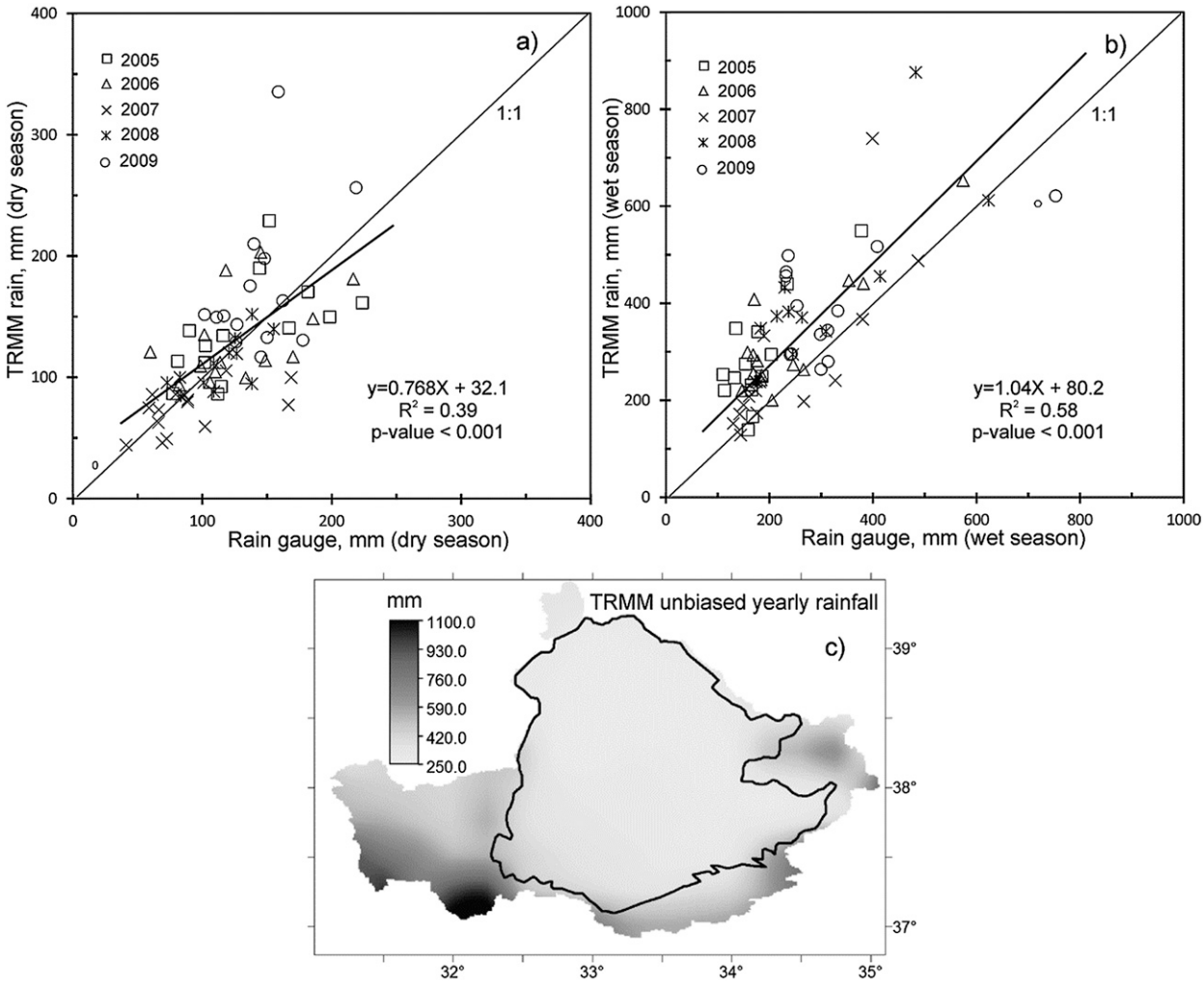

FIG. 7. (a),(b) The comparison of TRMM seasonal rainfall with ground-based rain gauge measurements in the dry (April–September) and wet seasons (October–March), respectively, and (c) the distribution of average unbiased yearly TRMM rainfall in the Konya basin (2005–09). The outline delineates the plain areas from mountainous areas.

SEBS-SM models for the Konya basin. The two models give similar results in the ''wet'' areas such as the mountainous upstream areas in the southwest and east (outside the polygon in Fig. 9), in the irrigated croplands in the plain areas (see the land cover map in Fig. 12c), and in the water bodies and wetlands, where water (soil moisture) limitation on ET is not relevant. However, the two models are quite different in the ''dry'' areas (nonirrigated parts inside the polygon), where water limitation on ET is more important.

Table 2 summarizes the comparison of the yearly ET estimates by SEBS and SEBS-SM for different land cover types in the basin. According to Table 2, the yearly ET estimated by SEBS-SM was lower for all the land covers in the basin. The difference varied among the land covers: 50–60 mm lower in shrub, forest, and water body land covers; 90–100 mm lower in wetland and irrigated croplands; and 150–160 mm lower in nonirrigated croplands, sparse vegetation, pasture, and grassland land covers on average.

c. *Surface runoff generation and its redistribution*

Figure 10 shows the distribution of the average wet season excess $P_{wet} - ET_{wet}$ during the study period (2005–09) in the Konya basin. Based on the outflows (R) from the Beysehir and Yesildere subbasins (Fig. 10) and applying Eq. (3), we found an average surface water ratio (SW_{ratio}) of 0.4, ranging between 0.25 and 0.55 depending on the year of assessment (Fig. 11a). According to Fig. 11b, the surface water generation ranged from 100 to 400 mm yr^{-1} in the mountainous source areas (2005–09). Finally, Figs. 11c and 11d show the distributions of the

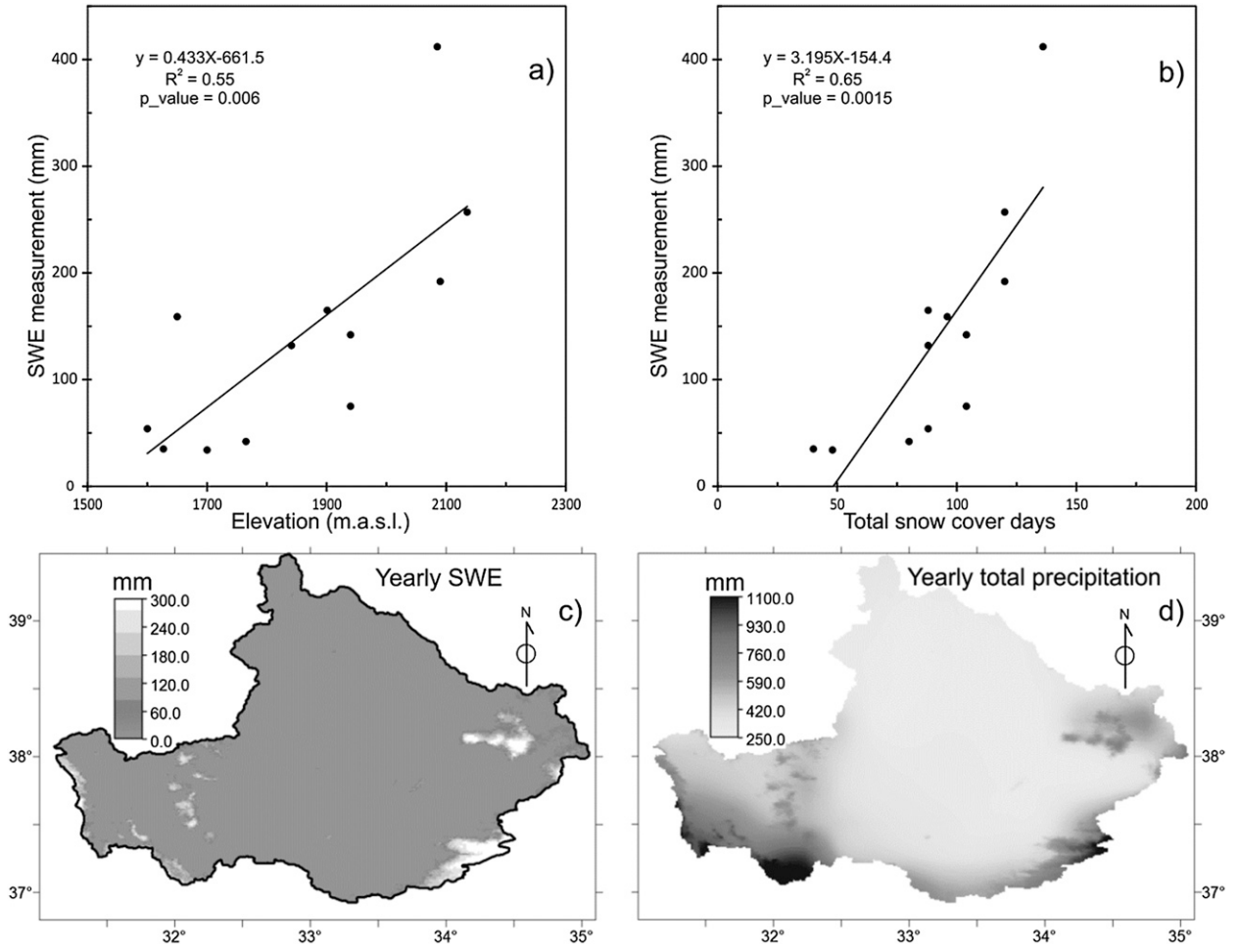

FIG. 8. (a),(b) Dependence of yearly SWE measurements on elevation and total snow cover days (source: MOD10A2 product), respectively, (c) the yearly SWE map, and (d) the yearly total precipitation map. Data of year 2008 were used in all the figures.

modified P_{wet} and P_{dry}, respectively, when the SW sources in Fig. 11b were subtracted from P_{wet} and then redistributed evenly over the irrigated pixels in P_{dry} (inside the irrigated croplands polygons in Fig. 11d based on land cover map). As a result, a range between 29 mm (2007) and 92 mm (2009) of SW irrigation was added per irrigated pixel for the study period (2005–09).

d. Spatially distributed water balance

1) DISTRIBUTION OF WATER LIMITATION AND *P*–ET ANOMALY

We first analyzed the degree of water limitation in the Konya basin by way of estimating aridity ratio of precipitation to potential evapotranspiration (*P*/PET), as shown in Fig. 12a. Based on the criterion for the water-limited environments (P/PET < 0.75) defined by Parsons and Abrahams (1994) we can say that except for the upstream mountainous parts in the southwest, south, and east, the whole Konya plain (indicated by the outline in Figs. 12a,b) can be classified as a highly water-limited environment with a *P*/PET ratio of about 0.3.

The next step was to quantify the spatial distribution of *P*–ET, where positive values ($P >$ ET) indicate potential for surface runoff and/or for GW recharge, while negative values ($P <$ ET) indicate actual consumption of supplementary water resources. In Fig. 12b, the large *P*–ET deficit (negative values) mainly corresponds to the irrigated croplands where irrigation water is used from groundwater and/or surface water sources. The irrigation water usage (the gross from surface and groundwater) for 2005–09, within the water-limited Konya plain (inside the outline in Fig. 12a), ranged up to $-500\,\text{mm yr}^{-1}$ and had a mean of $-308\,\text{mm yr}^{-1}$. Additionally, large *P*–ET deficit values occurred in lakes and wetlands, indicating significant groundwater and/or surface water inflow. In particular, the mean yearly *P*–ET deficit was −495 mm over the water bodies

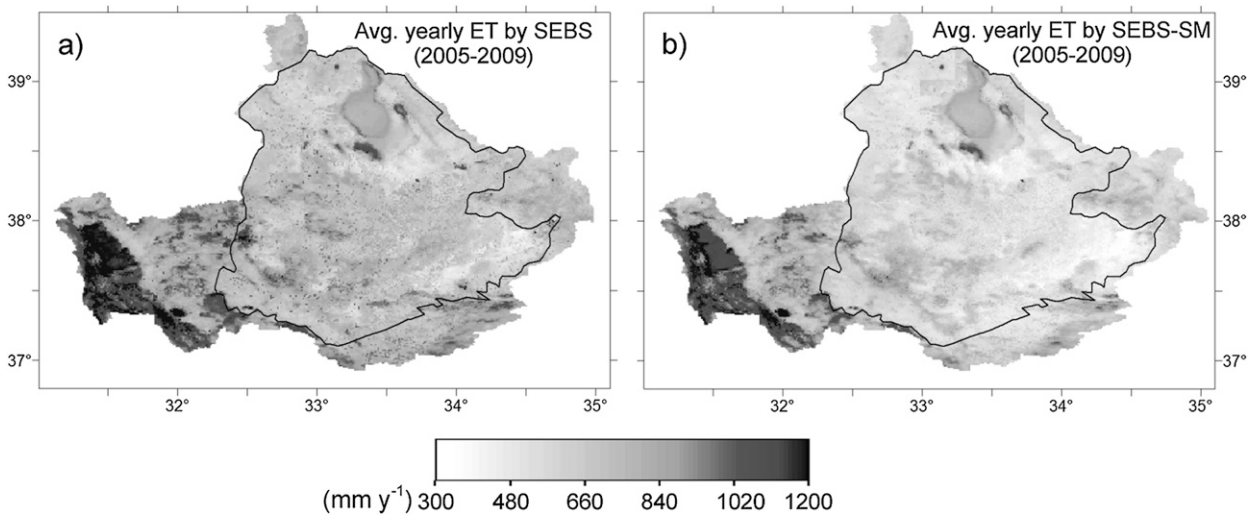

FIG. 9. Average yearly ET during the study period (2005–09) by (a) the original SEBS (Su 2002) and (b) the modified SEBS-SM (Gokmen et al. 2012).

(−600 mm in the freshwater Lake Beysehir in the southwest; −475 mm in the hypersaline Tuz Lake in the north) and −422 mm for the wetlands.

The *P*–ET surplus (positive values in Fig. 12b) was on the order of 300 mm yr^{-1} and occurred mainly in the mountainous upstream areas in the southwest and southeast where considerable surface runoff generation and/or GW recharge took place. According to the histogram of the *P*–ET for the whole basin (Fig. 12d), the majority of pixels have a negative balance with a mean *P*–ET of −238 mm yr^{-1}.

Table 3 provides a summary of the yearly *P*, ET, and (*P*–ET) fluxes in the water-limited Konya plain. The average yearly total storage change (*P*–ET) for the whole Konya plain is about −8500 million cubic meters (MCM) (−270 mm yr^{-1}). In the case of croplands, the mean *P*–ET deficits are −308 and −230 mm yr^{-1} for irrigated and nonirrigated croplands respectively, with a total volume of around −4700 MCM yr^{-1} together. Although the mean *P*–ET deficit for nonirrigated crops is considerably lower than for irrigated crops, −230 mm yr^{-1} still indicates considerable ET excess in nonirrigated agricultural lands. The smallest yearly *P*–ET deficit occurred in the sparse steppe vegetation (average −209 mm yr^{-1}), which is still around 70% in excess of the total *P* influx.

2) DISTRIBUTION AND CLOSURE OF WATER BALANCE

Figure 13 shows both the records of five GW observation wells (Figs. 13a–d) and the yearly water balance ($P \pm R - ET$) (Fig. 13e), which includes redistribution of the surface water (*R*) originated from wet season precipitation in the mountainous areas, over the irrigated areas of the Konya plain in dry season (Fig. 13e) as schematically presented in Fig. 5b. The groundwater observation wells Fethiye and Batum are located in the oldest irrigation region of the Konya basin. According to first-degree linear least squares fitting, groundwater level in these wells showed a negative slope of −0.3 m yr^{-1} (decreasing trend) between 1978 and 2004 (Fig. 13c), whereas after 2004 an even steeper

TABLE 2. Comparison of the average yearly ET (2005–09) estimated by SEBS and SEBS-SM in the Konya basin; note that the aerial percentages of the land covers do not sum up to 100% since only the major land cover units are considered.

Unit	Flux	Area (%)	Avg. yearly ET (mm)	Std. dev. (mm)
Konya basin	SEBS	100	772	155.2
	SEBS-SM		647.2	176.9
Irrigated croplands	SEBS	16.2	736.2	111.9
	SEBS-SM		632.2	118.2
Nonirrigated croplands	SEBS	21.5	709.7	93.7
	SEBS-SM		558.2	92.2
Mixed croplands	SEBS	7.0	648.3	162.1
	SEBS-SM		767.5	142.7
Wetland	SEBS	1.2	798.5	197.3
	SEBS-SM		708.9	219.2
Sparse steppe vegetation	SEBS	12.9	802.8	162
	SEBS-SM		644.2	185.7
Pasture and grassland	SEBS	15.0	731.1	125.4
	SEBS-SM		578.9	130.5
Shrub	SEBS	4.7	964.5	152.1
	SEBS-SM		900.3	167.6
Forest	SEBS	1.1	1,046	151.9
	SEBS-SM		998.4	156.9
Water body	SEBS	2.9	983.5	202.3
	SEBS-SM		922.2	206.3

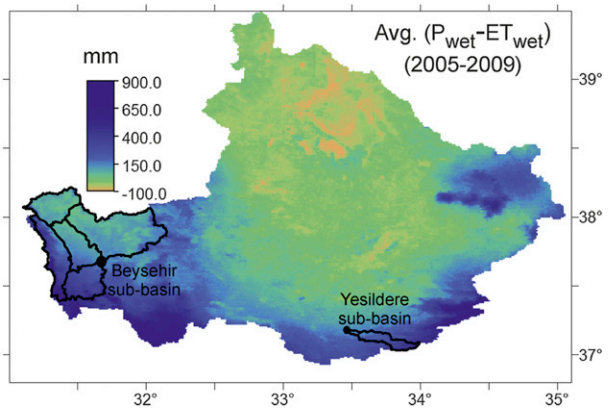

FIG. 10. The distribution of the average $P_{wet} - ET_{wet}$ during the study period (2005–09) including the locations of Lake Beysehir and Yesildere subbasins.

negative slope than $-2\,m\,yr^{-1}$ is observed. According to the hydrogeological report by DSI, most of the aquifers in the Konya plain are confined due to a thick layer of Pliocene sandy clay deposits (Fig. 5) but the degree of confinement is variable. The two other wells on irrigated fields (Tutup and Gulfet yayla; Figs. 13a,d) also indicate a large negative slope of around $1\,m\,yr^{-1}$ after the mid-1990s.

In Fig. 13, both the RS-based water balance estimation and the records of GW observation wells indicated widespread and varying degree of decrease in the storage. To be able to check if the water budget can be really closed at the locations (pixels) of the GW observation wells, we compared the average yearly ΔS_{RS} estimates from the RS-based water balance ($P \pm R - ET$) with the average ΔS_{GW} ranges for the five monitored wells in the period between 2005 and 2009 (Table 4 and Fig. 14).

According to Table 4 and Fig. 14a, the average yearly storage change (ΔS_{RS}) estimated from the RS-based water balance falls within the range of ΔS_{GW} constrained by a karst specific yield S_y range of 0.05–0.20, with the exception of Sigircik well. Figure 14a and Table 4 also show that the relative magnitudes match well: the highest storage changes (both ΔS_{RS} and ΔS_{GW}) are observed for the Batum and Fethiye wells ($\Delta S_{RS} = -409$

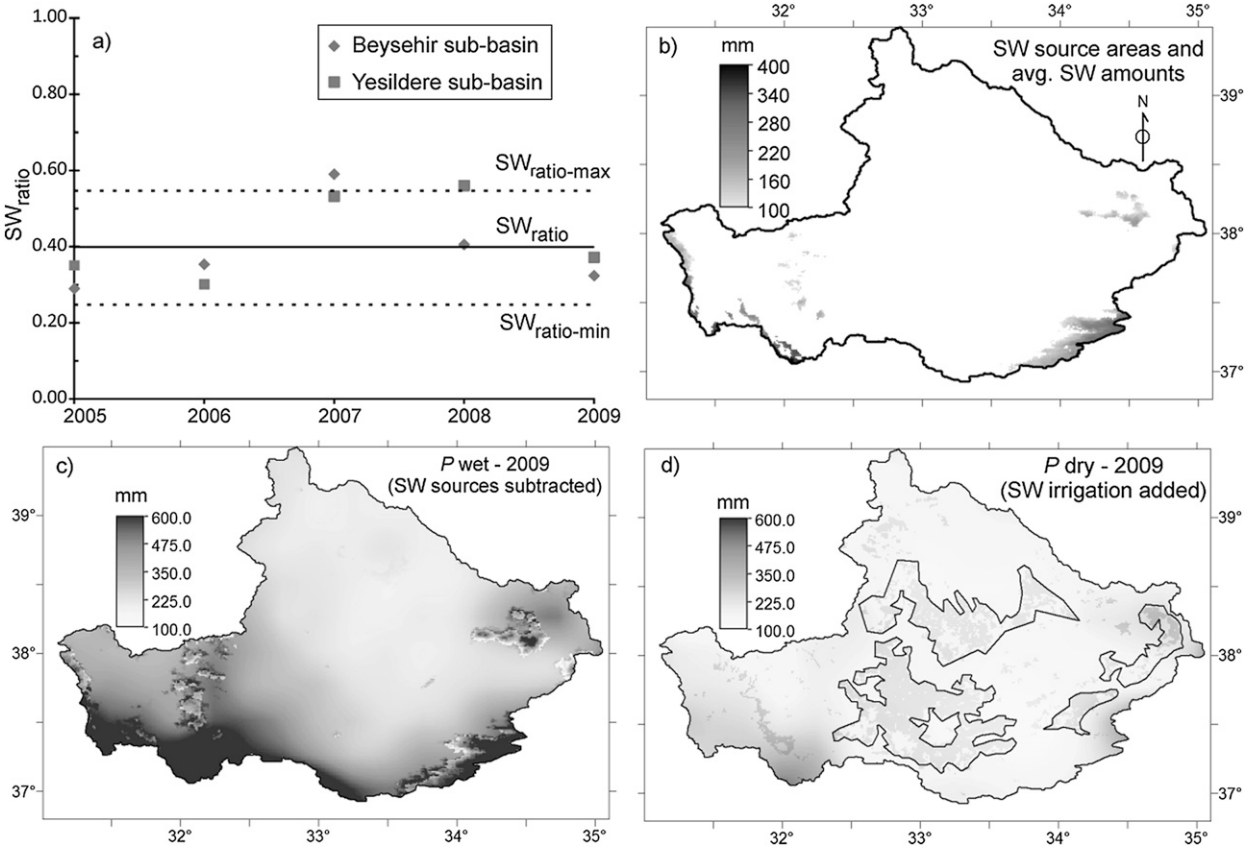

FIG. 11. Assessment of supplementary SW irrigation: (a) average, yearly changes, and standard deviations of the SW_{ratio} in Lake Beysehir and Yesildere subbasins; (b) distribution of the surface water source areas and quantities identified from ($P_{wet} - ET_{wet}$); (c) P_{wet} after transferring (subtracting) the generated surface water; and (d) P_{dry} after transferring in the surface water as irrigation within the delineated polygons of the plain area. Note that (b) represents the average of the study period (2005–09); (c) and (d) represent the year 2009.

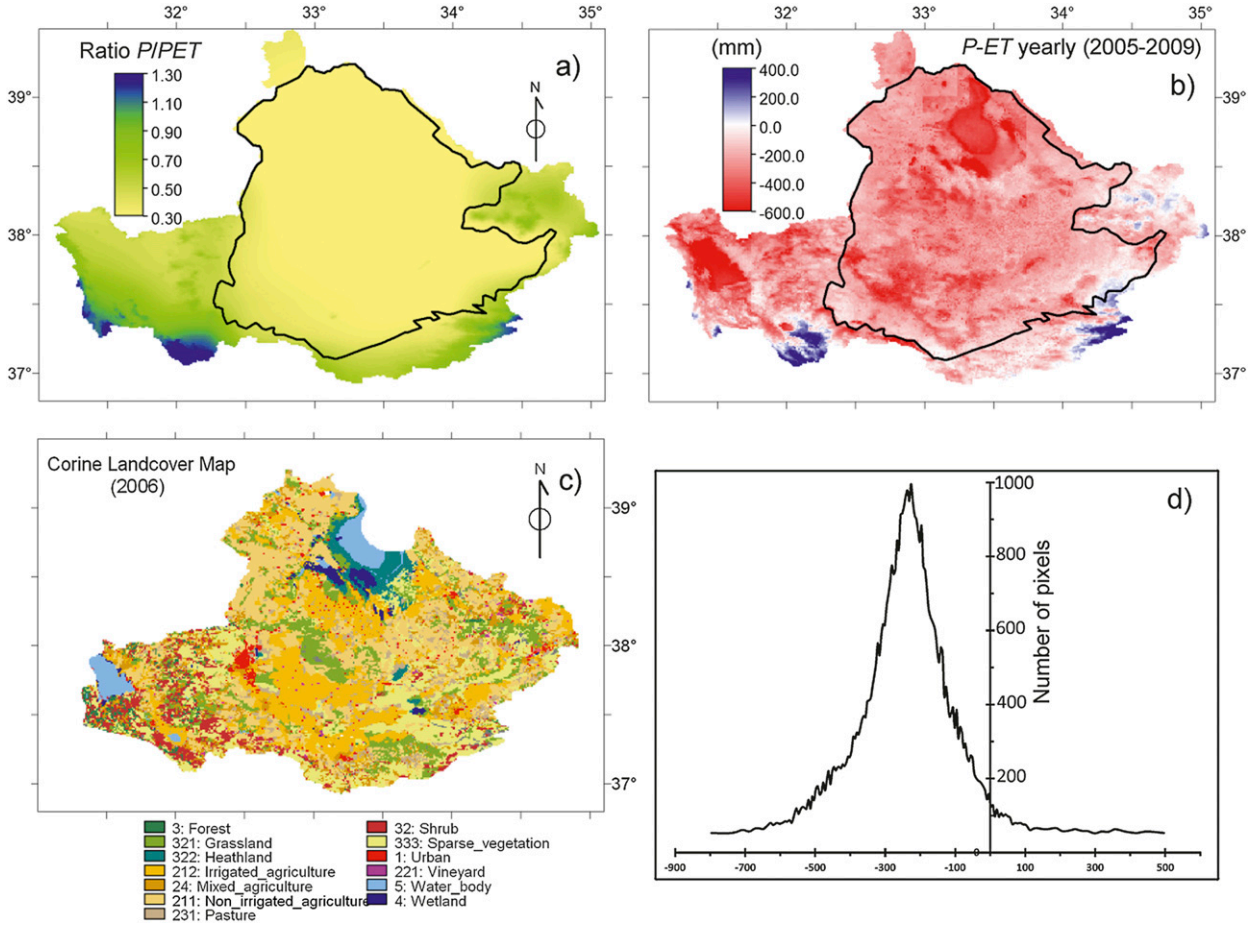

FIG. 12. (a) Water limitation as defined by the P/PET ratio; (b) $P - \mathrm{ET}$ in the Konya basin; (c) CORINE land cover map (source: Ministry of Environment of Turkey); (d) histogram of $P - \mathrm{ET}$.

and $-335\,\mathrm{mm\,yr^{-1}}$, respectively), while the lowest storage changes are observed for the Sigircik and Gulfet yayla wells ($\Delta S_{\mathrm{RS}} = -227$ and $-238\,\mathrm{mm\,yr^{-1}}$, respectively). Figures 14b–f show the yearly comparison between the ΔS_{RS} and the ΔS_{GW} at each monitoring well during the study period.

4. Discussion

It is an increasing trend to use RS data and RS-based models in hydrological research, but they still have their drawbacks, among others, in accuracy, difficulties in validation, scale issues, and spatial and temporal resolution limitations. Studies of Sheffield et al. (2009), Gao et al. (2010), and Sahoo et al. (2011) evaluated water budget closure in major river basins using RS data and they all concluded that achieving budget closure from remote sensing only is not possible yet. They indicated that the largest uncertainties were found in satellite precipitation products. On the other hand, a global-scale ET study by Vinukollu et al. (2011) concluded that the three RS-based ET models they tested (including SEBS) underrepresent the sensitivity to soil moisture over water-limited regions.

Our study is similar to those studies in utilizing RS-based estimates of P and ET to obtain a distributed water balance. However, the current study differs first in that instead of a purely RS-based approach (e.g., Sheffield et al. 2009; Sahoo et al. 2011; Armanios and Fisher 2013), we followed an integrated approach combining RS and ground-based methods. Second, we evaluated the budget closure of a spatially distributed water balance again in a spatially distributed manner by comparing the storage change inferred as the residual of the water balance with the distributed GW level observations, not in a lumped way (e.g., Armanios and Fisher 2013). Furthermore, as it was applied in a semiarid closed basin where limited water resources (both surface and groundwater) are strongly affected by human interaction, our study focused on the ways of improving

TABLE 3. Summary of the average yearly ET and *P* fluxes (2005–09) in the Konya plain; note that the aerial percentages of the land covers do not sum up to 100% since only the major land cover units are considered.

Unit	Flux	Area (%)	Avg. (mm)	Std. dev. (mm)	Total vol. (MCM)
Konya plain	*P*	100	306	59	9711
	ET		576	115	18 296
	P − ET		−270	189	−8585
Irrigated crops	*P*	23.2	313	49	2312
	ET		622	112	4586
	P − ET		−308	132	−2274
Nonirrigated crops	*P*	34.1	313	68	3393
	ET		544	82	5894
	P − ET		−231	91	−2499
Wetland	*P*	1.7	262	19	140
	ET		683	206	365
	P − ET		−422	209	−225
Sparse steppe vegetation	*P*	9.0	299	46	853
	ET		508	99	1451
	P − ET		−210	92	−598
Pasture and grass	*P*	16.8	306	56	1627
	ET		534	88	2840
	P − ET		−228	92	−1213
Shrub	*P*	0.4	395	119	55
	ET		756	147	105
	P − ET		−361	119	−50
Water body	*P*	2.7	266	22	224
	ET		761	75	642
	P − ET		−495	76	−418

P and ET estimations under semiarid conditions through integrating different data/methods (i.e., RS and ground) and introducing the most up-to-date models.

a. Improvement of P and ET fluxes

With respect to improving the estimate of the distribution of *P*, there were two steps: bias removal of RS rainfall products, and integration of SWE contribution to the total precipitation. First, we assessed the monthly product TRMM (3B43). Similar to Pan et al. (2008), who reported a positive bias in TRMM monthly rainfall product, we have also detected a positive bias of around 80 mm by the TRMM monthly product in the Konya basin. Furthermore, a separate analysis of wet and dry periods showed that the bias was consistent in the wet season (October–March) but not in the dry season (April–September). We argue that such a seasonal difference can be attributed to the higher magnitude of rainfall and also to the dominance of frontal type of rains during the wet season, compared to the spatiotemporally scattered convective rains in the dry season.

Second, since the bias correction was based on rain gauges located at relatively low altitudes, the TRMM product contains only negligible snowfall information in the mountainous areas. Furthermore, the number of in situ snowpack measurement sites is very low (Serreze et al. 1999). Possibilities of SWE measurements from RS is limited (Tang et al. 2010) and in any case the available RS products from microwave sensors are known to be less accurate in regions of complex terrain due to slope aspect and the limitations from the instantaneous field of view of the sensors, which can cause underestimations on mountains of complex geometry (Muskett 2012). Therefore, alternatively we applied a multiregression approach using the snow-gauge measurements, DEM and RS-based snow cover data, to obtain the distribution of the yearly SWE in the Konya basin. While snow cover data are an indispensable variable to identify snow occurring areas, it has long been known that topography plays important physical roles in influencing the magnitude of precipitation (Muskett 2012). Our results indicated that snowfall can contribute up to 25%–30% (~300 mm SWE) of total yearly precipitation in the higher altitudes of upstream areas (> 2000 m MSL in the Konya basin) that is neglected by the TRMM precipitation estimates. Therefore, we suggest including the SWE of the snowpack in the precipitation distribution to avoid serious underestimation of *P* in high-altitude terrain, where major surface water generation and groundwater recharge are occurring.

With respect to improving distribution of ET under semiarid conditions, our study applied a modified version of the SEBS model (SEBS-SM) that explicitly incorporates soil moisture information in the calculation. With that model we have overcome the problems of nonsensitivity of previous RS-based ET models to soil moisture over water-limited regions as indicated by the studies of Vinukollu et al. (2011), van der Kwast et al. (2009), and Lubczynski and Gurwin (2005). Principally, as it was put forward by the conceptual model of Seneviratne et al. (2010), lowering of soil moisture has a decreasing effect on the evaporative fraction (the portion of available energy spent for evapotranspiration) due to greater stomatal control on the water use by plants and increasing soil resistance to evaporation under water-stress conditions (Gokmen et al. 2012). Along these lines, this study showed quantitatively that the integration of soil moisture in SEBS-SM had a lowering effect in the estimation of yearly ET compared to SEBS in the water limited Konya basin. That magnitude of lowering was proportional to the aridity of the area (mean ≈ −120 mm, minimum ≈ 0 mm, maximum ≈ −400 mm), being the largest in the regions under the strongest water stress areas (Fig. 9)—that is, in the plain areas with low *P* values (~250–400 mm; Fig. 8d) and no supplementary water input (i.e., irrigation or groundwater discharge).

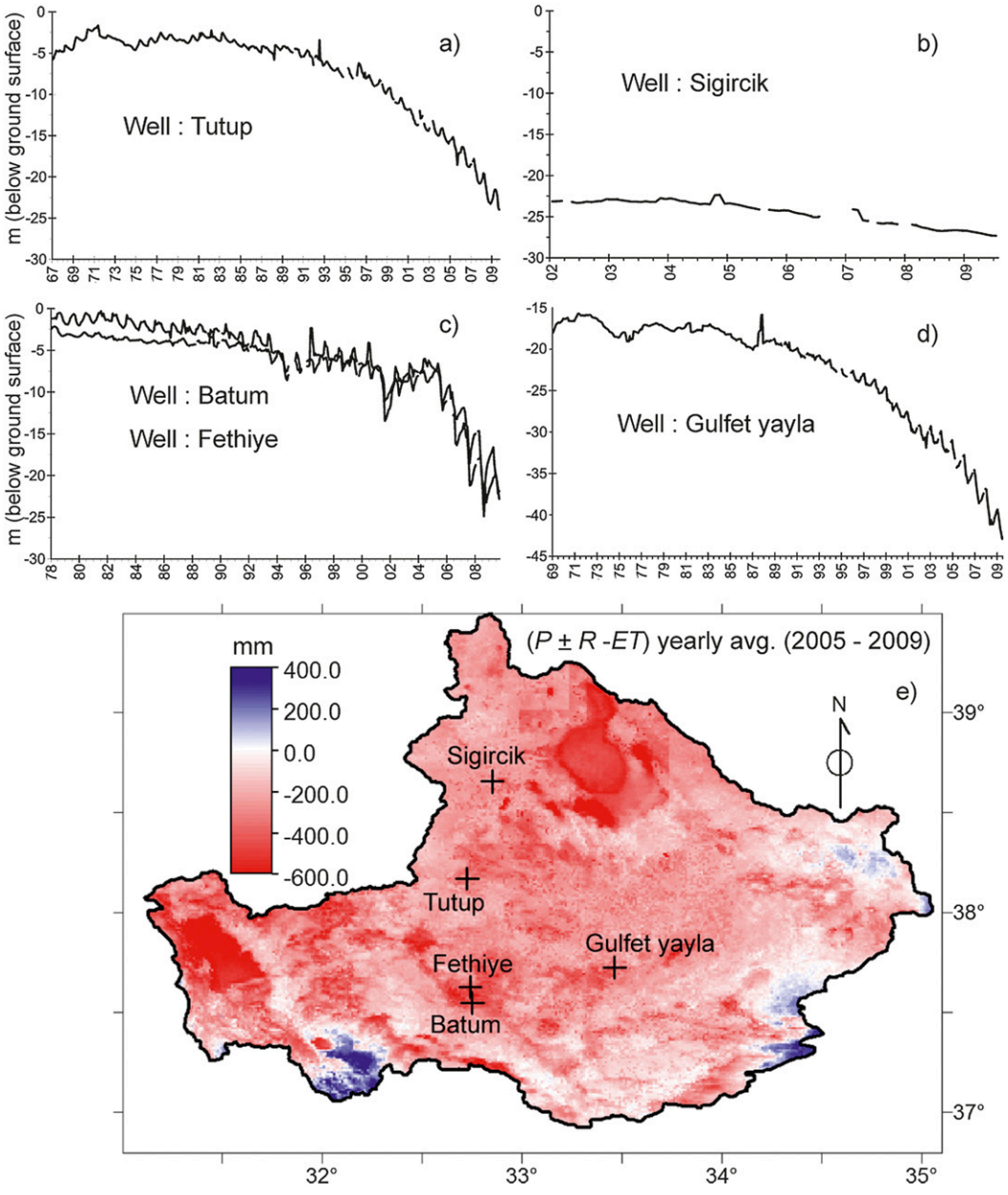

FIG. 13. Trends in groundwater observation wells and the net spatially distributed water balance map ($P + R - \mathrm{ET}$).

b. Distribution of P–ET anomaly, water balance, and budget closure

After obtaining improved distributions of the yearly P and ET in the Konya basin, we assessed P–ET anomalies, storage change as the residual of the water budget equation ($P \pm R - \mathrm{ET}$, or ΔS), and finally the budget closure at the locations of groundwater level observations. As defined by Contreras et al. (2011), areas with excess of P over ET generate surface runoff or GW recharge to the aquifers, while excess of ET over P results in the consumption of supplementary water resources (i.e., direct use of phreatic groundwater, groundwater discharge to a wetland, natural surface water contributions, and water withdrawal for irrigation). In the Konya basin, the distribution of P–ET and the water balance ($P \pm R - \mathrm{ET}$, or ΔS) indicated that there was widespread negative water balance (i.e., negative storage change) of varying magnitude during the study period of 2005–09. These negative water balance values can be mainly related to the enhancement of ET by the extensive and intensive agricultural activities

TABLE 4. Comparison between the effective GW loss observations from the field data and the average yearly water balance ($P + R - \mathrm{ET}$) estimated by RS-based methods for several locations in the Konya basin during the study period (2005–09).

		Field data		RS estimation
Name of GW well	S_y (specific yield)	Avg. GW level change ($\mathrm{mm\,yr^{-1}}$) 2005–09	Effective GW change, ΔS_{GW} ($\mathrm{mm\,yr^{-1}}$) 2005–09	$(P + R - \mathrm{ET})$ ΔS_{RS} ($\mathrm{mm\,yr^{-1}}$) 2005–09
Sigircik	0.05–0.2	−750	−37.5 to −150	(255.4 + 0.0 − 482.4) −227.0
Tutup		−1560	−78 to −312	(294.5 + 62.5 − 650.3) −293.3
Batum		−2870	−143.5 to −574	(364.4 + 62.5 − 836.2) −409.3
Fethiye		−2170	−108.5 to −434	(349.3 + 62.5 − 746.4) −334.6
Gulfet yayla		−1890	−94.5 to −378	(284.4 + 62.5 − 585.3) −238.4

stimulated by supplementary groundwater use for irrigation purposes. The largest negative *P*–ET values were found over water bodies and wetlands, suggesting these ecosystems are highly dependent on the groundwater (and/or surface water) inputs to sustain the excess ET (Table 3).

Afterward, to assess the budget closure at the locations (pixels) of GW observation wells, ΔS_{RS} values estimated from RS ($P \pm R - \mathrm{ET}$) were compared with the ΔS_{GW} calculated based on yearly groundwater decline and it was found that the average yearly ΔS_{RS} values were within the ranges of ΔS_{GW} for four of a total of five wells estimated assuming an S_y range between 0.05 and 0.20. These findings suggest that that RS-based estimate of ΔS_{RS} was capable of obtaining the magnitude and distribution of the groundwater storage depletion in the semiarid Konya basin, which had also been reported by Bayari et al. (2009). A similar approach was also documented by Tang et al. (2010) but our study differs in that we validated the spatially distributed water balance directly with GW level observations, whereas they validated their satellite-based water balance against the streamflow data at two river basins.

c. *Evaluation of the error sources and the uncertainties*

Despite the effectiveness of the RS-based $P \pm R - \mathrm{ET}$ in capturing groundwater depletion reflected by storage change, estimation of each water balance flux component separately and the methodology of the spatiotemporal water balance assessment are still prone to a variety of error sources and uncertainties. First, the Coordinate Information on the Environment (CORINE) land cover map (Fig. 12c) used in analyzing the land cover–based ET and *P* fluxes was originally rasterized from a polygon map and resampled to 1-km resolution. Because of rather coarse spatial resolution (1 km), this procedure was vulnerable to the mixed-pixel effect (i.e., ET and *P* fluxes were likely to represent a mixture of different land cover types). Still, one would expect that the long-term yearly averages of *P* and ET in relatively flat terrain with little surface runoff should be in a similar range for land covers like sparse steppe vegetation. Despite the fact that the smallest yearly *P*–ET difference occurred in sparse steppe vegetation (average $\approx -209\,\mathrm{mm\,yr^{-1}}$), the yearly ET was still around 70% in excess of the total *P* influx. The large difference can mainly be attributed to the low value of *P* in the Konya plain ($\sim 300\,\mathrm{mm\,yr^{-1}}$), which causes higher relative uncertainty per unit absolute error for low values of *P*. Our comparison of the TRMM rainfall product with the rain gauges showed a significant positive bias ($p < 0.001$) in the wet season and the correlation coefficient was not high ($R^2 = 0.58$), implying that the magnitude of bias varies considerably among the stations and years of the study period (Fig. 7b). In response to that, we subtracted a bias of ~80 mm from the yearly *P* before the analysis. Such a bias removal had relatively more influence and uncertainty in the plain, low *P* areas as compared to mountainous, high *P* areas.

Despite the improvements by SEBS-SM in representing the ET in water-limited environments, Gokmen et al. (2012) reported an overall relative error (rRMSE) of 26% SEBS-SM (which was originally 36% for SEBS) by comparing its output with observations from the Bowen ratio stations installed in in the Konya basin. It should be noted that even ground-based flux measurements derived from Bowen ratio and eddy covariance systems have an uncertainty of around 20%–30% (Kalma et al. 2008, and references therein). Besides the uncertainties in estimating the daily ET, the process of filling the data gaps in daily ET values for obtaining monthly and yearly ET is also prone to uncertainties that have been the subject of several studies (e.g., Anderson et al. 2012; Delogu et al. 2012; Ferguson et al. 2010; Gao et al. 2006). In effort to further minimize the errors in estimating the monthly and the yearly ET, an option was to densify and extend the samples (i.e., more frequent RS flux estimations in a longer study period). Therefore, we ran SEBS-SM on a daily interval for a 5-yr

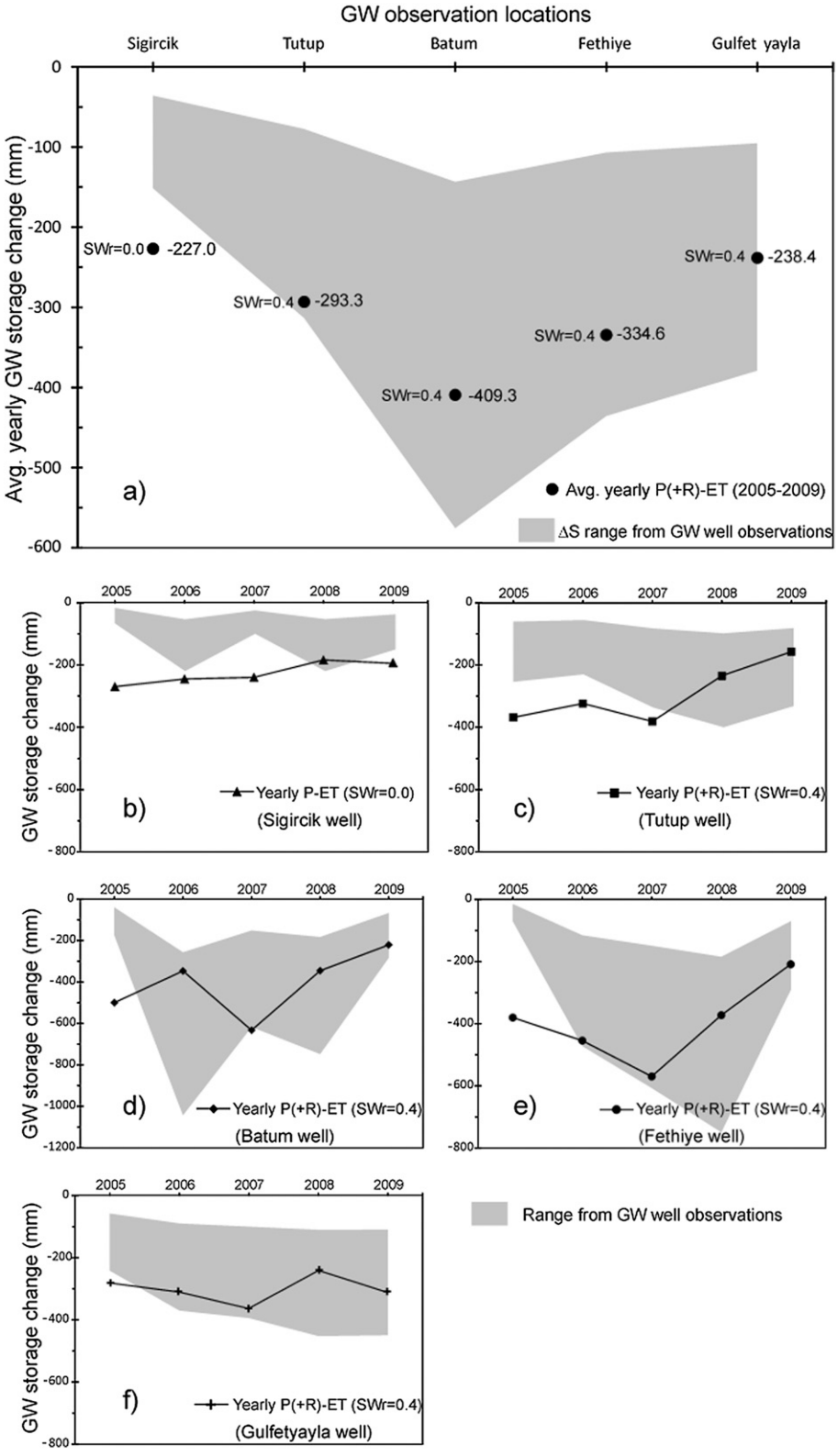

FIG. 14. Comparison between the RS-based change of storage ($\Delta S = P + R - \mathrm{ET}$) and the change of GW storage based on the observation wells, showing (a) the yearly average of the study period (2005–09) and (b)–(f) yearly changes for each monitoring well. [Note that SW irrigation (R) was estimated separately for each year.]

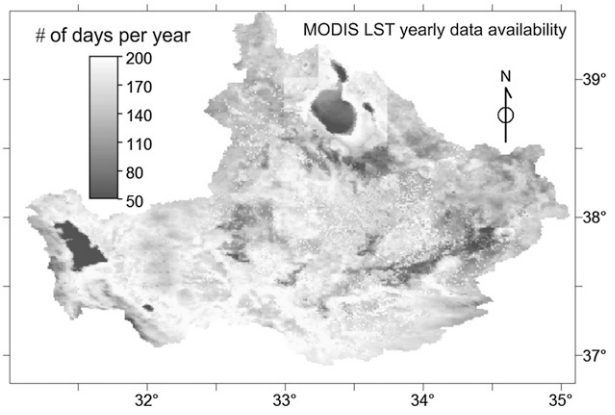

FIG. 15. The distribution of the average number of days that the MODIS land surface temperature (LST) data were available during the study period in the Konya basin.

study period between 2005 and 2009. However, as shown in Fig. 15, the RS data availability varied largely in the Konya basin due to weather variations and to the data quality policy applied by the MODIS team on certain variables such as land surface temperature or emissivity variables. Comparing the data availability (Fig. 15) with the land cover map of Fig. 12c, we can conclude that there was a generally good data availability (on average about 200 days per year in 2005–09) for the croplands, while the availability was generally lower (50–100 days per year) for the natural steppe vegetation (sparse vegetation and pasture areas), mountainous upstream areas, and water bodies. This can be attributed to the higher cloud coverage in the mountainous areas and the higher uncertainties in the calculation of emissivity especially for the sparsely vegetated areas. In fact, in contrast to those data-sparse areas, we can claim lower uncertainties in quantifying the yearly ET for data-intensive areas such as croplands, which is supported by the general agreement between the ΔS_{RS} estimates and the ΔS_{GW} from the groundwater level observations in Table 4 and Fig. 14.

Finally, besides the uncertainties in quantifying the individual fluxes, there are also some methodological uncertainties in comparing ΔS_{RS} and ΔS_{GW}. First, there is a difference in terms of representativeness. The ΔS_{RS} estimated by RS methods represents the whole storage change beneath the surface (soil moisture in the unsaturated zone, GW in the saturated zone), while the measurements of the GW level change represent only the GW storage change. To minimize the effect of the variations in soil moisture in the unsaturated zone (ΔS_{SM}), we used an extended study period of 5 yr, which helped to balance out the variations in ΔS_{SM} and ΔS_{RS} estimation to primarily represent changes in the groundwater storage. Second, not only the uncertainty of ΔS_{RS} but also the uncertainty of the ΔS_{GW} plays a role in explaining some of the misfit between ΔS_{RS} and ΔS_{GW} (Figs. 14b–f). The ΔS_{GW} value is dependent on the accuracy of the S_y estimate, which for karstic rocks is highly uncertain (due to the unpredictable type and degree of karstification) so it could even be beyond the variability range defined in this study. In fact, it is shown in Fig. 14 that the uncertainty of ΔS_{GW} due to the uncertainty of specific yield (gray shaded area) was considerable. In addition, assigning a spatially constant SW_{ratio} that is estimated in a few selected subcatchments of the mountainous areas represents a simplification because the mountainous areas are heterogeneous and the SW_{ratio} can vary with different altitude, topography, soil type, vegetation, etc. However, according to our testing of the different SW_{ratio} ranges given in Fig. 11a, the effect of varying SW_{ratio} on R and thereby on ΔS_{RS} (i.e., $P \pm R - ET$) was low compared to the effect of S_y on ΔS_{GW} because the contribution of SW was only ~20% to the total water use (i.e., irrigation) in the Konya basin, which is highly groundwater dependent (Table 4).

5. Conclusions

In this study, we aimed at developing a method for improved RS-based estimations of yearly P, ET, and R water fluxes for evaluation of the storage changes in the water-limited Konya basin in a distributed manner. For assessing the effectiveness of the methodology, we compared the results with groundwater storage changes estimated by water table decline in boreholes. The proposed methodology relies on the integrated assessment (i.e., RS and ground methods) of individual fluxes. Important aspects in the assessment of P are 1) the correction of the TRMM rainfall product with ground-based rainfall estimates in gauges and 2) an estimate of snowfall contribution to precipitation from the SWE of the snowpack based on RS and field measurements. The assessment of ET confirmed the advantage of SEBS-SM over the standard SEBS by its better accounting for the water stress conditions (i.e., soil moisture limitation on ET), which was reflected as estimating a lower yearly ET compared to SEBS with varying magnitude. The supplementary SW transfer for irrigation (R) from mountainous areas to lowland plain areas was defined as the product of the SW_{ratio} representing surface water outflow characteristic of the mountainous areas and the RS-defined water surplus $P_{wet} - ET_{wet} > 0$. The mean SW irrigation estimated during the 5 years of the study period was 63 mm yr^{-1} (~20% of total irrigation), which is well in agreement with the estimate by the local water authority. The remaining 80% of the irrigation was originated from groundwater. The overall irrigation

(estimated as P–ET deficit) from the irrigated croplands was found to reach up to $-500\,\mathrm{mm\,yr^{-1}}$ (with a mean of $-308\,\mathrm{mm\,yr^{-1}}$) with a total volume change of $-2270\,\mathrm{MCM\,yr^{-1}}$ (total = $-4700\,\mathrm{MCM\,yr^{-1}}$ for all croplands) in the study period (2005–09). The maximum yearly P–ET differences were observed for wetland (average $-422\,\mathrm{mm\,yr^{-1}}$) and water bodies (average $-495\,\mathrm{mm\,yr^{-1}}$), showing that they receive large groundwater and/or surface water inputs to sustain such excess ET.

In the water-limited conditions of arid and semiarid regions where absolute values of water fluxes are low, the same level of absolute error as in water-abundant areas translates into relatively larger uncertainty. In an effort to minimize that uncertainty, we employed the strategy of a frequent and long period of ET flux estimations (i.e., 5 yr with daily time step of SEBS-SM). This particularly helped to reduce the uncertainty of the yearly ET, especially in data-intensive areas (Fig. 15). The comparison of the RS-based change of storage (ΔS_{RS}) with the change of groundwater storage (ΔS_{GW}) showed that 1) there was better agreement between the ΔS_{RS} and ground-based ΔS_{GW} when analyzing the 5-yr period than while analyzing yearly data because the 5-yr data were less affected by yearly unsaturated storage changes; 2) the yearly changes and patterns of ΔS_{RS} and ΔS_{GW} were similar; and 3) the ΔS_{GW} uncertainty due to the uncertainty of S_y was significant and mainly resulted from the highly heterogeneous and unpredictable karst aquifer.

Our study showed that RS-based P and ET estimates are capable of estimating the spatially distributed water balance and storage changes with good accuracy in a large semiarid basin. The proposed method can also be applied in other large basins, especially in semiarid and arid regions, where there are higher potentials for obtaining long time series of frequent optical remote sensing data. The yearly ET estimations can still be improved in RS data-scarce areas (e.g., high cloud coverage areas) by using radar/microwave RS in ET estimation (no limitation of clouds). Furthermore, more advanced RS-based precipitation products will help further reduce the uncertainties in quantifying the spatially distributed water balance. The RS-based spatiotemporally distributed water balance solutions, as presented in this study, can be very useful for water managers as well as for agricultural, climate, and ecohydrological studies, among others, and provide an assessment type that could not be feasible using point-based ground measurements.

Acknowledgments. We thank Prof. Dr. Hasan Z. Sarıkaya for his support for the realization of the research, especially with regards to field studies.

We also thank the staff of the Regional Water Authority (DSI 4 Bölge Müdürlüğü), especially Mr. Mehmet Demirel, Mr. Kemal Olgun, and Mr. Adnan Başaran for their help in carrying the fieldwork and providing the groundwater data, and to Mr. Yücel Kaya for providing the snow observation data.

REFERENCES

Alsdorf, D. E., and D. P. Lettenmaier, 2003: Tracking fresh water from space. *Science,* **301,** 1491–1494, doi:10.1126/science.1089802.

Anderson, M. C., R. G. Allen, A. Morse, and W. P. Kustas, 2012: Use of Landsat thermal imagery in monitoring evapotranspiration and managing water resources. *Remote Sens. Environ.,* **122,** 50–65, doi:10.1016/j.rse.2011.08.025.

Armanios, D. E., and J. B. Fisher, 2013: Measuring water availability with limited ground data: Assessing the feasibility of an entirely remote-sensing-based hydrologic budget of the Rufiji Basin, Tanzania, using TRMM, GRACE, MODIS, SRB, and AIRS. *Hydrol. Processes,* doi:10.1002/hyp.9611, in press.

Bayari, C., N. Ozyurt, and S. Kilani, 2009: Radiocarbon age distribution of groundwater in the Konya Closed Basin, central Anatolia, Turkey. *Hydrogeol. J.,* **17,** 347–365, doi:10.1007/s10040-008-0358-2.

Biancamaria, S., N. Mognard, A. Boone, M. Grippa, and E. Josberger, 2008: A satellite snow depth multi-year average derived from SSM/I for the high latitude regions. *Remote Sens. Environ.,* **112,** 2557–2568, doi:10.1016/j.rse.2007.12.002.

Bolster, C. H., D. P. Genereux, and J. E. Saiers, 2001: Determination of specific yield for the Biscayne Aquifer with a canal-drawdown test. *Groundwater,* **39,** 768–777, doi:10.1111/j.1745-6584.2001.tb02368.x.

Brunner, P., P. Bauer, M. Eugster, and W. Kinzelbach, 2004: Using remote sensing to regionalize local precipitation recharge rates obtained from the chloride method. *J. Hydrol.,* **294,** 241–250, doi:10.1016/j.jhydrol.2004.02.023.

Chang, A. T. C., J. L. Foster, R. E. J. Kelly, E. G. Josberger, R. L. Armstrong, and N. M. Mognard, 2005: Analysis of ground-measured and passive-microwave-derived snow depth variations in midwinter across the northern Great Plains. *J. Hydrometeor.,* **6,** 20–33, doi:10.1175/JHM-405.1.

Contreras, S., E. G. Jobbágy, P. E. Villagra, M. D. Nosetto, and J. Puigdefábregas, 2011: Remote sensing estimates of supplementary water consumption by arid ecosystems of central Argentina. *J. Hydrol.,* **397,** 10–22, doi:10.1016/j.jhydrol.2010.11.014.

Delogu, E., and Coauthors, 2012: Reconstruction of temporal variations of evapotranspiration using instantaneous estimates at the time of satellite overpass. *Hydrol. Earth Syst. Sci.,* **16,** 2995–3010, doi:10.5194/hess-16-2995-2012.

Derksen, C., P. Toose, A. Rees, L. Wang, M. English, A. Walker, and M. Sturm, 2010: Development of a tundra-specific snow water equivalent retrieval algorithm for satellite passive microwave data. *Remote Sens. Environ.,* **114,** 1699–1709, doi:10.1016/j.rse.2010.02.019.

Ferguson, C. R., J. Sheffield, E. F. Wood, and H. L. Gao, 2010: Quantifying uncertainty in a remote sensing-based estimate of evapotranspiration over continental USA. *Int. J. Remote Sens.,* **31,** 3821–3865, doi:10.1080/01431161.2010.483490.

Fontugne, M., C. Kuzucuoglu, M. Karabiyikoglu, C. Hatté, and J. F. Pastre, 1999: From Pleniglacial to Holocene: A C-14 chronostratigraphy of environmental changes in the Konya Plain, Turkey. *Quat. Sci. Rev.,* **18,** 573–591, doi:10.1016/S0277-3791(98)90098-1.

Gao, F., J. Masek, M. Schwaller, and F. G. Hall, 2006: On the blending of the Landsat and MODIS surface reflectance: predicting daily Landsat surface reflectance. *IEE Trans. Geosci. Remote. Sens.,* **44,** 2207–2218, doi:10.1109/TGRS.2006.872081.

Gao, H., Q. Tang, C. R. Ferguson, E. F. Wood, and D. P. Lettenmaier, 2010: Estimating the water budget of major US river basins via remote sensing. *Int. J. Remote Sens.,* **31** (14), 3955–3978, doi:10.1080/01431161.2010.483488.

Ghilain, N., A. Arboleda, and F. Gellens-Meulenberghs, 2011: Evapotranspiration modelling at large scale using near-real time MSG SEVIRI derived data. *Hydrol. Earth Syst. Sci.,* **15,** 771–786, doi:10.5194/hess-15-771-2011.

Gleeson, T., J. VanderSteen, M. A. Sophocleous, M. Taniguchi, W. M. Alley, D. M. Allen, and Y. X. Zhou, 2010: Groundwater sustainability strategies. *Nat. Geosci.,* **3,** 378–379, doi:10.1038/ngeo881.

Gokmen, M., Z. Vekerdy, A. Verhoef, W. Verhoef, O. Batelaan, and C. van der Tol, 2012: Integration of soil moisture in SEBS for improving evapotranspiration estimation under water stress conditions. *Remote Sens. Environ.,* **121,** 261–274, doi:10.1016/j.rse.2012.02.003.

Green, T. R., M. Taniguchi, H. Kooi, J. J. Gurdak, D. M. Allen, K. M. Hiscock, H. Treidel, and A. Aureli, 2011: Beneath the surface of global change: Impacts of climate change on groundwater. *J. Hydrol.,* **405,** 532–560, doi:10.1016/j.jhydrol.2011.05.002.

Huffman, G. J., and D. T. Bolvin, 2013: TRMM and other data precipitation data set documentation. NASA, 40 pp. [Available online at ftp://precip.gsfc.nasa.gov/pub/trmmdocs/3B42_3B43_doc.pdf.]

——, and Coauthors, 2007: The TRMM multisatellite precipitation analysis (TMPA): Quasi-global, multiyear, combined-sensor precipitation estimates at fine scales. *J. Hydrometeor.,* **8,** 38–55, doi:10.1175/JHM560.1.

Jia, L., and Coauthors, 2003: Estimation of sensible heat flux using the Surface Energy Balance System (SEBS) and ATSR measurements. *Phys. Chem. Earth,* **28,** 75–88, doi:10.1016/S1474-7065(03)00009-3.

Jin, X., M. E. Schaepman, J. G. P. W. Clevers, and Z. B. Su, 2009: Impact and consequences of evapotranspiration changes on water resources availability in the arid Zhangye Basin, China. *Int. J. Remote Sens.,* **30,** 3223–3238, doi:10.1080/01431160802559053.

Johnson, A. I., 1967: Specific yield—Compilation of specific yields for various materials. Geological Survey Water Supply Paper 1662-D, 74 pp.

Joyce, R. J., J. E. Janowiak, P. A. Arkin, and P. P. Xie, 2004: CMORPH: A method that produces global precipitation estimates from passive microwave and infrared data at high spatial and temporal resolution. *J. Hydrometeor.,* **5,** 487–503, doi:10.1175/1525-7541(2004)005<0487:CAMTPG>2.0.CO;2.

Kalma, J. D., T. R. McVicar, and M. F. McCabe, 2008: Estimating land surface evaporation: A review of methods using remotely sensed surface temperature data. *Surv. Geophys.,* **29,** 421–469, doi:10.1007/s10712-008-9037-z.

Lubczynski, M. W., and J. Gurwin, 2005: Integration of various data sources for transient groundwater modeling with spatio-temporally variable fluxes—Sardon study case, Spain. *J. Hydrol.,* **306,** 71–96, doi:10.1016/j.jhydrol.2004.08.038.

Ma, W., M. Hafeez, U. Rabbani, H. Ishikawac, and Y. Ma, 2012: Retrieved actual ET using SEBS model from Landsat-5 TM data for irrigation area of Australia. *Atmos. Environ.,* **59,** 408–414, doi:10.1016/j.atmosenv.2012.05.040.

Ma, Y., M. Song, H. Ishikawa, K. Yang, T. Koike, L. Jia, M. Menenti, and Z. Su, 2007: Estimation of the regional evaporative fraction over the Tibetan plateau area by using Landsat-7 ETM data and the field observations. *J. Meteor. Soc. Japan,* **85A,** 295–309, doi:10.2151/jmsj.85A.295.

McCabe, M. F., E. F. Wood, R. Wójcik, M. Pan, J. Sheffield, H. Gao, and H. Su, 2008: Hydrological consistency using multi-sensor remote sensing data for water and energy cycle studies. *Remote Sens. Environ.,* **112,** 430–444, doi:10.1016/j.rse.2007.03.027.

Muskett, R. R., 2012: Multi-satellite and sensor derived trends and variation of snow water equivalent on the high-latitudes of the northern hemisphere. *Int. J. Geosci.,* **3,** 1–13, doi:10.4236/ijg.2012.31001.

Naing, Z. W., 2011: Groundwater fluxes in the Konya closed basin, Turkey. M.S. thesis, Water Resources Department, University of Twente, 55 pp.

Oku, Y., H. Ishikawa, and Z. B. Su, 2007: Estimation of land surface heat fluxes over the Tibetan Plateau using GMS data. *J. Appl. Meteor. Climatol.,* **46,** 183–195, doi:10.1175/JAM2456.1.

Owe, M., R. de Jeu, and T. Holmes, 2008: Multisensor historical climatology of satellite-derived global land surface moisture. *J. Geophys. Res.,* **113,** F01002, doi:10.1029/2007JF000769.

Pagano, T. C., and S. Sorooshian, 2006: Global water cycle (fundamental, theory, mechanisms). *Encyclopedia of Hydrological Sciences,* Vol. 5, M. G. Anderson and J. J. McDonnell, Eds., Wiley, 2697–2711.

Pan, M., E. F. Wood, R. Wójcik, and M. F. McCabe, 2008: Estimation of regional terrestrial water cycle using multi-sensor remote sensing observations and data assimilation. *Remote Sens. Environ.,* **112,** 1282–1294, doi:10.1016/j.rse.2007.02.039.

——, A. K. Sahoo, T. J. Troy, R. K. Vinukollu, J. Sheffield, and E. F. Wood, 2012: Multisource estimation of long-term terrestrial water budget for major global river basins. *J. Climate,* **25,** 3191–3206, doi:10.1175/JCLI-D-11-00300.1.

Parsons, A. J., and A. D. Abrahams, 1994: Geomorphology of desert environments. *Geomorphology of Desert Environments,* A.D. Abrahams and A.J. Parsons, Eds., CRC Press, 1–12.

Penck, A., 1896: Unterschungen über Verbunstung und Abfluss von grösseren Landflächen. *Geogr. Abh.,* **5,** 5.

Prigent, C., F. Chevallier, F. Karbou, P. Bauer, and G. Kelly, 2005: AMSU—A land surface emissivity estimation for numerical weather prediction assimilation schemes. *J. Appl. Meteor.,* **44,** 416–426, doi:10.1175/JAM2218.1.

Sahoo, A. K., M. Pan, T. J. Troy, R. K. Vinukollu, J. Sheffield, and E. F. Wood, 2011: Reconciling the global terrestrial water budget using satellite remote sensing. *Remote Sens. Environ.,* **115,** 1850–1865, doi:10.1016/j.rse.2011.03.009.

Seneviratne, S. I., T. Corti, E. L. Davin, M. Hirschi, E. B. Jaeger, I. Lehner, B. Orlowsky, and A. J. Teuling, 2010: Investigating soil moisture-climate interactions in a changing climate: A review. *Earth Sci. Rev.,* **99,** 125–161, doi:10.1016/j.earscirev.2010.02.004.

Serreze, M. C., M. P. Clark, R. L. Armstrong, D. A. McGinnis, and R. S. Pulwarty, 1999: Characteristics of the Western United States snowpack from snowpack telemetry (SNOTEL) data. *Water Resour. Res.,* **35,** 2145–2160, doi:10.1029/1999WR900090.

Sheffield, J., C. R. Ferguson, T. J. Troy, E. F. Wood, and M. F. McCabe, 2009: Closing the terrestrial water budget from satellite remote sensing. *Geophys. Res. Lett.,* **36,** L07403, doi:10.1029/2009GL037338.

Snyder, R. L., M. Orang, S. Matyac, and M. E. Grismer, 2005: Simplified estimation of reference evapotranspiration from pan evaporation data in California. *J. Irrig. Drain. Eng.,* **131,** 249–253, doi:10.1061/(ASCE)0733-9437(2005)131:3(249).

Su, H., M. F. McCabe, E. F. Wood, Z. Su, and J. H. Prueger, 2005: Modeling evapotranspiration during SMACEX: Comparing two approaches for local- and regional-scale prediction. *J. Hydrometeor.,* **6,** 910–922, doi:10.1175/JHM466.1.

Su, Z., 2002: The Surface Energy Balance System (SEBS) for estimation of turbulent heat fluxes. *Hydrol. Earth Syst. Sci.,* **6,** 85–99, doi:10.5194/hess-6-85-2002.

——, and Coauthors, 2010: Earth observation Water Cycle Multi-Mission Observation Strategy (WACMOS). *Hydrol. Earth Syst. Sci. Discuss.,* **7,** 7899–7956, doi:10.5194/hessd-7-7899-2010.

Swenson, S., and J. Wahr, 2002: Methods for inferring regional surface-mass anomalies from Gravity Recovery and Climate Experiment (GRACE) measurements of time-variable gravity. *J. Geophys. Res.,* **107,** 2193, doi:10.1029/2001JB000576.

Tang, Q., H. Gao, P. Yeh, T. Oki, F. Su, and D. P. Lettenmaier, 2010: Dynamics of terrestrial water storage change from satellite and surface observations and modeling. *J. Hydrometeor.,* **11,** 156–170, doi:10.1175/2009JHM1152.1.

van der Kwast, J., and Coauthors, 2009: Evaluation of the Surface Energy Balance System (SEBS) applied to ASTER imagery with flux-measurements at the SPARC 2004 site (Barrax, Spain). *Hydrol. Earth Syst. Sci.,* **13,** 1337–1347, doi:10.5194/hess-13-1337-2009.

Vinukollu, R. K., E. F. Wood, C. R. Ferguson, and J. B. Fisher, 2011: Global estimates of evapotranspiration for climate studies using multi-sensor remote sensing data: Evaluation of three process-based approaches. *Remote Sens. Environ.,* **115,** 801–823, doi:10.1016/j.rse.2010.11.006.

Wada, Y., L. P. H. van Beek, and M. F. P. Bierkens, 2012: Nonsustainable groundwater sustaining irrigation: A global assessment. *Water Resour. Res.,* **48,** W00L06, doi:10.1029/2011WR010562.

Wahr, J., S. Swenson, and I. Velicogna, 2006: Accuracy of GRACE mass estimates. *Geophys. Res. Lett.,* **33,** L06401, doi:10.1029/2005GL025305.

Yeh, P. J.-F., S. C. Swenson, J. S. Famiglietti, and M. Rodell, 2006: Remote sensing of groundwater storage changes in Illinois using the Gravity Recovery and Climate Experiment (GRACE). *Water Resour. Res.,* **42,** W12203, doi:10.1029/2006WR005374.